To the Graduate Council :

I am submitting herewith a dissertation written by Ida Lee entitled "Desorption of Metal Atoms and Large Molecules by Laser Induced Surface Plasmons." I have examined the final copy of this dissertation for form and content and recommend that it be accepted in partial fulfillment of the requirements for the degree of Doctor of Philosophy, with a major in Physics.

T. A. Callcott

Thomas A. Callcott, Major Professor

We have read this dissertation
and recommend its acceptance :

E. T. Arakawa

Jau-shyong Lin

Accepted for the Council :

Lew Minkel

Vice Provost
and Dean of The Graduate School

DESORPTION OF METAL ATOMS AND LARGE MOLECULES BY LASER INDUCED SURFACE PLASMONS

A Dissertation

Presented for the

Doctor of Philosophy

Degree

The University of Tennessee, Knoxville

Ida Lee

May 1991

ABSTRACT

Surface plasmons excited by a Nd:YAG laser in an attenuated-total-reflection (ATR) geometry were used to desorb Al, Au, Ag atoms, and rhodamine B molecules. The metal films were vacuum-evaporated on glass prisms while the rhodamine B film was deposited on an Al film. The desorbed neutrals were ionized by a XeCl excimer laser and measured by a time-of-flight mass spectrometer. The desorption yield exhibits a sharp maximum at the surface-plasmon resonance angle. The kinetic energy (KE) distributions of the desorbed particles were obtained by varying the delay time between the two lasers. For all the metals, there were one low energy peak and one high energy peak in the KE distribution. The low energy peak was identified as a thermal peak. The high energy peak was identified by further experiments and calculations as electronic-excited desorption. Rhodamine B molecules were desorbed by this method without fragmentation. Finally, we discussed the possible desorption mechanisms and gave reasons for our conclusion.

TABLE OF CONTENTS

CHAPTER

I. INTRODUCTION 1

A. PREVIOUS WORK 1

B. SCOPE OF THIS WORK 6

II. THEORY 9

A. ABSORPTION OF LASER LIGHT 9

B. MECHANISM OF DESORPTION 17

III. EXPERIMENTAL METHODS 23

A. EXPERIMENTAL APPARATUS 23

B. EXPERIMENTAL PROCEDURES 26

IV. RESULTS AND COMPARISONS 30

A. DESORPTION OF METAL FILMS 30

B. DESORPTION OF RHODAMINE B 36

V. DISCUSSION AND CONCLUSION 39

A. SUMMARY OF RESULTS 39

B. DISCUSSION 41

APPENDIX 47

REFERENCES 79

VITA 85

LIST OF FIGURES

FIGURE PAGE

2-1. Surface plasmon dispersion relation (SP) for a free-electron metal 48

2-2. Principle of the optical excitation of surface plasmon by attenuated total reflection (ATR) in the Kretschmann configuration 49

2-3. Reflectance R as a function of incidence angle 50

2-4. Energy densities of the electromagnetic field from laser light at different incidence angles 51

2-5. Menzel, Gomer, and Redhead (MGR) model of electronic-excited desorption 52

3-1. Schematic of the time-of-flight mass spectrometer (TOF-MS) 53

3-2. Arrangement for desorption experiment 54

3-3. Schematic of the ATR geometry in our experiment 55

3-4. Schematic of the data acquisition electronics 56

4-1. Desorption yields from Al film at various angles of incidence 57

FIGURE PAGE

4-2. Comparison between desorption yield A-1 and energy absorbed by the Al film at various angles..... 58

4-3. Dependence of Al desorption yield on laser power..... 59

4-4. Kinetic energy distribution of Al atoms desorbed from Al film..... 60

4-5. Comparison between desorption yield from Au and calculated energy absorbed by the Au film at various angles..... 61

4-6. Kinetic energy distribution of Au atoms desorbed from Au film..... 62

4-7. Delay time distribution for low energy peak of Au..... 63

4-8. Temperature variation of thermal peak with laser fluence..... 64

4-9. Comparison between desorption yield from Ag and calculated energy absorbed by the Ag film at various angles..... 65

4-10. Kinetic energy distribution of Ag atoms desorbed from Ag film..... 66

4-11. Molecular structure of rhodamine B..... 67

FIGURE PAGE

4-12. Desorption yields from rhodamine B molecules adsorbed on an Al film at various angles of incidence with laser fluence 210 mJ/cm^2 68

4-13. Desorption yields from rhodamine B molecules adsorbed on an Al film at various angles of incidence with laser fluence 178 mJ/cm^2 69

5-1. Electromagnetic energy density profile of Al film 70

5-2. Electromagnetic energy density profile of Au film 71

5-3. Electromagnetic energy density profile of Ag film 72

5-4. Comparison between desorption yield, total optical absorption, and energy density at metal-vacuum interface for the Al film 73

5-5. Comparison between desorption yield, total optical absorption, and energy density at metal-vacuum interface for the Au film 74

5-6. Comparison between desorption yield, total optical absorption, and energy density at metal-vacuum interface for the Ag film 75

CHAPTER I

INTRODUCTION

A. PREVIOUS WORK

Photodesorption by laser light has been used in recent years to produce well-defined microstructures[1,2] (*via* micromachining), to study high-T_c superconductors[3,4,5](*via* surface analysis), and to probe molecular dynamics in heterogeneous systems.[6,7,8] These processes have therefore been actively studied in the past and the studies are continuing with increasing sophistication.[9,10,11,12,13] Photodesorption of particles from a solid surface can be achieved by rapid surface heating,[14,15,16,17,18] by coupling to phonon modes,[19,20,21,22] and by coupling to electronic excitation processes.[23,24,25,26] These reactions usually are studied under high vacuum (HV) or ultra high vacuum (UHV) conditions with time-resolved optical spectroscopy or mass spectrometry.

In laser-induced thermal desorption (LITD), rapid surface heating can result from direct excitation of lattice phonons or from electronic excitations which subsequently decay to phonons. Many studies have been done which concern thermal effects on solids due to heating by laser light.[27,28,29]

Infrared (IR) lasers can be used to couple directly to the phonon modes including both the internal modes of the absorbate and the adsorbate-surface vibrational modes. The first report of resonant absorption of infrared photons by adsorbed molecules was made by Heidberg *et al.*[19,20] This desorption mechanism was reviewed by T.J. Chuang.[9,21] In practice

there is only a narrow range of laser fluence in which resonantly-excited desorption can be observed, so that other direct laser heating effects often overwhelm and wash out the resonant adsorbate excitation effect.

Relatively few reports have appeared on photodesorption induced by electronic excitation of surfaces by ultraviolet (UV) and visible lasers. Since the basic mechanism is nonthermal, it has drawn increasing interest in recent years. V.S. Antonov *et al*.[23] have observed nonthermal desorption of molecular ions of polyatomic molecules induced by UV laser radiation. Desorbed ions are found to have a non-thermal initial velocity distribution with an excess of ions with extremely high ejection speed.

Bourdon *et al*.[24] have reported that CH_3Br molecules adsorbed on a LiF crystal could be photodesorbed by an excimer laser at 222 or 308 nm. Their major finding is that electronic excitation of the adsorbate leads to photodissociation on a sufficiently short time scale that the dynamics is obviously different from laser-induced thermal desorption (LITD). These two different pathways, LITD and electronic desorption, give rise to desorbed products with different peak energies (E) and energy widths (ΔE). For electronic-excited photodissociation the radical CH_3 is ejected with E = 1.5 eV and ΔE = 0.6 eV, and for LITD the molecule CH_3Br is ejected with E =0.060 eV and ΔE = 0.14 eV.

K. Domen *et al*.[25,30] chose CH_2I_2 molecules adsorbed on Al_2O_3 (sapphire crystal) and Ag (film) surfaces as a model system to examine laser excited surface processes in the UV. The time-of-flight (TOF) signals of CH_2I radicals produced from laser excitation of CH_2I_2 adsorbed on Al_2O_3 were observed. At surface coverages of a monolayer or less ($\Theta \leq 1$), the yield

increases linearly with fluence (F) from 0 to 500 mJ/cm^2. The peak position and shapes of TOF signals remain the same with F up to 500 mJ/cm^2. The mean kinetic energy (KE) of desorbed ions is E = 0.095 eV. Their results clearly reveal a characteristic electronic desorption effect. When F > 500 mJ/cm^2, the LITD becomes significant. For CH_2I_2 adsorbed on an Ag film with $\Theta \leq 1$, no desorption signal was detected until F > 50 mJ/cm^2. At the coverage $2 \leq \Theta \leq 10$, the KE ($E \approx 0.095$ eV) of CH_2I is independent of F, again showing the characteristic electronic effect. When $F \geq 80$ mJ/cm^2, laser-induced substrate heating becomes important. Since the quantum yield for dissociation is very low (0.01 - 0.1), the electronic relaxation of the excited adsorbate is apparently rather rapid on both Al_2O_3 and Ag surfaces.

F. Budde *et al*.[26] have reported on the first full state-resolved (i.e. translational, rotational, vibrational, and spin level distributions) results for molecules photochemically desorbed from a well-defined surface. They have identified two desorption channels, thermal and nonthermal (electronic excitation), for NO molecules desorbed from an oxygen-covered Ni (100) surface by UV laser radiation (λ = 193 nm). The velocity distribution of these two groups of molecules have average values of $E/2k$ = 1010 °K and 250 °K (k is the Boltzmann's constant), respectively. The nonthermal part exhibits very strong spin-orbit selectivity at low rotational quantum numbers.

Photodesorption of molecules from metal surfaces irradiated by UV or visible lasers have been investigated by others also.[31,32,33,34] Quite often, nonthermal photodesorption characteristics are observed. These results suggested that direct electronic excitation of the adsorbed molecules is the major mechanism for photodesorption and photochemistry on the metal

surface. The rate of deexcitation by the metal surface is not sufficiently fast to quench the observed photochemistry. T.J. Chuang *et al*.[35] have shown that clean and effective photoetching of polymers PMMA (poly-methylmethacrylate), PMGI (poly-dimethyl-glutarimide), and CMS (chlorinated poly-methylstyrene) can be achieved by doping with pyrene molecules and ABH (4-aminobenzoylhydrazide) which can be electronically excited by 308 nm laser light. Charge transfer interactions between the excited dopant and the monomer units of the polymer might enhance the electronic excitation of the host polymer and thereby enhance its chemical decomposition.

H. Helvajian *et al*.[36] studied the ionic species ablated by laser light at very high fluences near the threshold for ion production. Their results reveal that for a crystalline silver target, the laser ablated ion products are ejected with kinetic energy E = 9 eV. The kinetic energies of the ejected ions (Ag^+, Ag_2^+, adsorbed Fe^+) do not vary with wavelength (351 nm and 248 nm), nor with the ion product mass, and within limits are independent of the laser fluence. However, the ion yield and dimer/monomer (Ag_2^+/Ag^+) ion ratio depend upon the laser wavelength. They believe the desorption is possibly induced by electronic transitions.

W. Hoheisel *et al*.[37,38,39] have observed that sodium (Na) atoms with energies of several electron-volts are ejected from small Na particles supported on a LiF single crystal if a surface-plasmon oscillation is excited with laser light. The desorption yield exhibits a dependence on the laser frequency with a maximum at λ = 490 nm for Na particles of 50 nm average radius. At the resonant frequency, the desorption rate depends linearly on

the cw laser irradiance in the range from about I = 40 mW/cm^2 up to 160 W/cm^2. A single peak is observed in the TOF mass spectrum, its position does not depend on the laser fluence. The position of the peak maximum corresponds to a kinetic energy of E = 1.64 eV. The effect is nonthermal and it appears that neutral atoms are desorbed after the collective electron oscillation decays into a repulsive single electron state. This study has particular relevance to our studies, which we believe demonstrate photodesorption associated with the excitation of surface plasmons.

Photodesorption of rhodamine ions has been investigated by S.V. Chekalin and V.S. Letokhov *et al.* [40,41,42]. They observed the photodesorption of rhodamine 6G ions adsorbed on the surface of tungsten and subjected to ultrashort (30 p sec) pulses of the second harmonic of a YAG:Nd laser, whose wavelength was λ = 532 nm and intensity 10^8 W/cm^2. Those ions were not desorbed by pulses of the λ = 1064 nm wavelength, which was outside the electronic absorption band of rhodamine 6G, when the intensity was increased up to 10^9 W/cm^2. When the target was irradiated at the 1064 nm wavelength, to which the rhodamine was essentially transparent, it resulted simply in heating of the substrate. Two peaks were observed under this condition and these were identified as Na and K. A comparison was made of the mass spectra obtained with thick rhodamine layers ($\geq 10^2$ monolayers) and thin rhodamine layers ($\leq$ one monolayer) irradiated at different laser wavelengths. The similarity of the mass spectra observed for a thick layer heated by the 1064 nm radiation and for a monolayer irradiated at 532 nm indicated that in both cases the appearance of ions was due to heating of the substrate. The absence of

photodetachment was associated with the rapid transfer of the electronic excitation from the adsorbed molecules to the electrons of the substrate metal. At the threshold I = 0.24 GW/cm^2 there was only one peak in the region of the molecular ions of rhodamine 6G when a thick layer was irradiated with laser wavelength λ = 532 nm. At laser intensities exceeding 0.3 - 0.5 GW/cm^2 the mass spectrum became very intense and broad, and peaks due to Na and K were also observed. This could be explained by the excitation of rhodamine molecules near the substrate and the transfer of excitation to K and Na impurity ions adsorbed on the substrate. When a thick layer was irradiated with the 4th harmonic (λ = 266 nm, inside the absorption band of rhodamine 6G), the mass spectra and their dependence on laser intensity were approximately the same as at λ = 532 nm. The thresholds for the appearance of rhodamine were the same at both wavelengths. They concluded that ultrashort pulses of 532 nm laser light can cause nonthermal desorption of rhodamine 6G molecular ions from a thick film without significant fragmentation of the molecules. This is attributed to collective processes of energy transfer in a layer of excited rhodamine molecules.

B. SCOPE OF THIS WORK

This work describes a promising new method of photodesorption[43] which greatly amplifies electronic field strength in the surface region, and discusses a few basic physical properties of the photodesorbed species which indicate that this method favors electronic over thermal processes. In

contrast to earlier work,[37,38,39] desorption in our experiment is stimulated by laser-induced surface plasmons in an attenuated-total-reflection (ATR) geometry. Since there is an enhancement of the electromagnetic field in the surface region when surface plasmons are stimulated, we are able to use low laser fluence to perform the electronic excited desorption. In the ATR geometry, photons can excite surface plasmons over a wide range of photon energies below the surface plasmon energy. Thus, compared with the work done by Hoheisel *et al*.[37,38,39] in which surface plasmons were excited over a narrow frequency range on rough surfaces, our experiment demonstrates that surface-plasmon-induced desorption can be accomplished on smooth surfaces over a wide range of wavelengths. This ability to tune the wavelength will be useful in studies of electronic desorption processes.

This dissertation is organized as follows. Chapter II is devoted to the fundamental theory behind the various laser-induced reactions. It deals primarily with the absorption and redistribution of the incident laser energy within the solid phase. Emphasis is placed on the interaction between the metal film and the electromagnetic field. Photon-stimulated excitation leading to desorption is also described. Both direct excitation by photons and excitation mediated by surface plasmons are discussed.

Chapter III describes our experimental apparatus and procedure. The experimental results from this work are reported in Chapter IV. We have measured desorption from Al, Au , and Ag films on SiO_2 substrates and from rhodamine B molecules on Al films. We report measurements of the dependence of the desorption rate on laser fluence, and on the degree of coupling of the laser light to the plasmon mode, and relate these results to

energy absorption in the film. In addition, we report measurements of the velocity distribution of desorbed atoms and molecules.

In Chapter V we summarize our results and discuss the various aspects of the experimental results.

CHAPTER II

THEORY

In this Chapter, we consider first the absorption of light in materials for the ATR geometry. The second section discusses desorption mechanisms.

A. ABSORPTION OF LASER LIGHT

Laser light, in order to cause any lasting effect on a material, must first be absorbed. Laser radiation from the ultraviolet to the infrared interacts primarily with the valence electrons of an atom or molecules, and sometimes, with a particular set of vibration modes, or phonons. The response of an optically excited material to laser radiation depends on its electronic configuration, its present state of matter (i.e. liquid, solid, vapor etc.), the atomic arrangement, and the nature of any other nearby species.

The response of nonferromagnetic, isotropic matter to an optical field may be described by two independent parameters at each wavelength or frequency (ω). In optics, these response parameters are often taken to be $n(\omega)$, the index of refraction, which provides a measure of the phase velocity of a propagating light wave in the medium, and $k(\omega)$, the extinction coefficient, which determines the exponential rate of damping of a wave by an absorption process. In electromagnetic theory, the two parameters are often described by the frequency dependent dielectric function $\varepsilon(\omega)$, which provides a measure of the polarization response of the medium, and $\sigma(\omega)$,

the optical conductivity, which provides a measure of energy absorption in the solid. In formulations of optical response theory utilizing complex functions these parameters are often described in terms of a complex index of refraction **n** and a complex dielectric function ε, where

$$\mathbf{n} = n + i\,k, \tag{2-1}$$

$$\varepsilon = \varepsilon_r + i\,\varepsilon_i = \varepsilon + i\,(2\pi\sigma/\omega). \tag{2-2}$$

The pairs of response functions are related by the equations

$$\varepsilon = \mathbf{n}^2, \tag{2-3}$$

$$\varepsilon_r = n^2 - k^2, \quad \varepsilon_i = 2\pi\sigma/\omega = 2nk. \tag{2-4}$$

For metal samples at the wavelength λ commonly used in laser desorption experiments (1.06 μm to 248 nm), excitation of conduction electrons is the primary absorption mechanism. Metals are characterized by their loosely-bound outermost electrons, which are free to travel from atom to atom. As a consequence of this behavior, the optical properties of most metals can be quite successfully described by the "free electron gas" model. In a free electron gas, a well-known classical analysis leads to a dielectric function of the form

$$\varepsilon = 1 - \frac{\omega_p^2}{\omega^2} \frac{1}{1 - \dfrac{1}{i\omega\tau}}, \tag{2-5}$$

where ω_p is the plasma frequency defined below, and τ is the relaxation time for electron scattering collisions. The real and imaginary parts of ε are given by

$$\varepsilon_r = 1 - \frac{\omega_p^2}{\omega^2} \frac{1}{1 + \dfrac{1}{\omega^2\tau^2}}, \tag{2-6}$$

$$\varepsilon_i = \frac{1}{\omega\tau}\,\frac{\omega_p^2}{\omega^2}\,\frac{1}{1+\frac{1}{\omega^2\tau^2}}\,, \qquad (2\text{-}7)$$

where $$\omega_p^2 = \frac{4\pi ne^2}{m^*}\,, \qquad (2\text{-}8)$$

and n, e, and m* are density, charge, and effective mass of the conduction electron, respectively.

For frequencies in the visible region and above, $\omega\tau >> 1$ so that the dielectric functions reduce to the simple forms

$$\varepsilon_r = 1 - \frac{\omega_p^2}{\omega^2}\,, \qquad (2\text{-}9)$$

$$\varepsilon_i = \frac{1}{\omega\tau}\,\frac{\omega_p^2}{\omega^2}\,. \qquad (2\text{-}10)$$

The plasma frequency is the resonance frequency for free oscillations of the negatively charged electron gas against a background of rigid positive charges. From Equations (2-9) and (2-10), these oscillations occur when

$$\varepsilon_r\,(\omega=\omega_p) = 0, \qquad (2\text{-}11)$$

$$\varepsilon_i\,(\omega=\omega_p) = 1/\omega\tau << 1. \qquad (2\text{-}12)$$

Since the electron gas is degenerate, only electrons in states close to the Fermi level contribute to the optical properties. From this approach, it follows that longitudinal density fluctuations, or plasma oscillations, will propagate through the volume of the metal. Bohm and Pines[44] first showed that longitudinal charge density waves with frequency ω_p propagate in the volume of a metal sample. The quanta of these "volume plasmons" have an energy $h\omega_p/2\pi$ of the order of 10 eV.

An important extension of the "volume plasmons" is the concept of "surface plasmons". Collective excitation of electrons exist not only in the

volume of a plasma but also in its boundary. Maxwell's theory shows that the electromagnetic surface waves can travel along a metallic surface or on metallic films. R. H. Ritchie *et al.* [45] first showed that charged density waves of lower frequency ω_s may propagate at an interface between a metal and insulating medium of dielectric function ε_0, when the dielectric function has the values

$$\varepsilon_r (\omega = \omega_s) = -\varepsilon_0 , \tag{2-13}$$

$$\varepsilon_i (\omega = \omega_s) << 1. \tag{2-14}$$

Longitudinal waves of the surface charge density propagate along the surface as a polarization wave of the form

$$\sigma (x, t) = \Delta\sigma \exp i (\omega t - k_x x), \tag{2-15}$$

where $k_x = 2\pi/\lambda$ is the wave vector of the propagating wave and $\Delta\sigma$ is the charge displacement in the surface at t =0 and x = 0. For a free-electron metal at a vacuum interface, this surface-plasmon frequency is

$$\omega_s = \frac{1}{\sqrt{2}} \omega_p , \tag{2-16}$$

where ω_p is the plasma frequency defined in Eq. (2-8). These surface plasmons can propagate along surfaces with a broad spectrum of eigenfrequencies from $\omega = 0$ up to $\omega = \omega_s$ depending on the wave vector **k**. The dispersion curve of ω vs. k for a free electron surface plasmon is shown in Fig. 2-1* along with the line characteristic of light propagating in vacuum. The surface plasmons have a longer wave vector than light waves of the

---

* All figures and tables are in the appendix.

same energy, $\hbar\omega/2\pi$, propagating along the surface. The excitation of surface plasmons by photons needs special photon-plasmon couplers (grating coupler, prism coupler), since the dispersion relation lies right of the light line, and ω and k for photons and plasmons do not overlap.

In real metals, interband transitions may strongly modify the free-electron dielectric functions and shift the plasmon frequencies far from the free-electron values given in Eq. (2-8) and Eq. (2-16). In such metals, volume and surface waves can be excited at the frequencies satisfying Eq. (2-11) and Eq. (2-12) for the volume wave and Eq. (2-13) and Eq. (2-14) for the surface wave. In particular, for Ag, a strong interband transition with onset at about 4 eV shifts the energies of the bulk (volume) and surface-plasmon oscillations to energies of 3.78 eV and 3.60 eV respectively. Plasma oscillations in real metals have been discussed in detail by Raether[46].

Surface plasmons can be excited on smooth surfaces by photons in an attenuated total reflection (ATR) configuration. This method was described by E. Kretschmann,[47] and this configuration is illustrated in Fig. 2-2. A thin film (medium 1) is deposited on a transparent prism or semicylinder (medium 0) of refractive index $n_0 = \sqrt{\varepsilon_0}$. P-polarized light (Electric field of the wave is parallel to the plane of incidence; often called the TM wave) incident through the prism has an electric field component parallel to the surface that can couple to the surface plasmon at a particular angle. Since the coupling occurs for angles above the angle for total internal reflection, $n_0 \sin\theta_0 = 1$, the film must be sufficiently thin so that the exponentially decaying

evanescent field can penetrate the film d, and excite the surface plasmon at the film/vacuum (1/2) interface.

The index n_0 decreases the photon wavevector at each ω, so that the light line within the prism ($\omega = \frac{c}{n_0} k$, c : velocity of light in vacuum, n_0 : refractive index of prism) has a smaller slope. Photon-plasmon coupling is accomplished when the parallel component of the photon wavevector (k_x) matches the surface plasmon wavevector

$$k_{sp} = k_x = n_0 \frac{\omega}{c} \sin \theta_0 , \qquad (2\text{-}17)$$

where θ_0 is the angle of incidence at the (0/1) interface. By varying θ_0, photon-plasmon coupling may be accomplished at all frequencies of the surface plasmon curve that lies to the left of the $\omega = \frac{c}{n_0} k$ light line. When surface plasmons are excited in this manner, the strong enhancement of the electromagnetic field in the surface is correlated with a strong reduction of the reflectance at the plasmon resonance angle. The reflected amplitude r is given by

$$r = \frac{r_{01} + r_{12} e^{i\beta}}{1 + r_{01} r_{12} e^{i\beta}} , \qquad (2\text{-}18)$$

where r_{01} and r_{12} are the (complex) Fresnel reflection coefficients for the p (TM) wave at the first and second interface, respectively. The change in phase of the beam on traversing the film is

$$\beta = \frac{2\pi}{\lambda} n_1 d \cos \theta_1 , \qquad (2\text{-}19)$$

where θ_1 is the (complex) angle of refraction in an absorbing medium (metal), n_1 is the complex index of refraction of the absorbing medium, d is the thickness of the absorbing medium, and λ is the wavelength of the

incident light. For angles beyond the critical angle and with no radiative de-excitation (*via* surface roughness, for instance), the transmitted energy is zero and the optical absorption is

$$A = 1 - R = 1 - |r|^2 . \qquad (2\text{-}20)$$

In Fig. 2-3, the reflectance $R = |r|^2$ is plotted as a function of incident angle for angles near the angle for photon-plasmon coupling. The optical constants for $\mathbf{n}_0$ and $\mathbf{n}_1$ are those appropriate for a glass prism ($n_0 = 1.517$, $k_0 = 0$) and for Al ($n_1 = 0.71$, $k_1 = 5.133$).

There is a strong enhancement of the electromagnetic field in at the metal/air interface (1/2) with the excitation of surface plasmons. The field intensity can be nearly 100 times stronger in resonance than out of resonance. The electromagnetic fields decay exponentially in both directions perpendicular to the surface and have their maximum in the surface, as is characteristic for surface waves.

We can evaluate the electromagnetic energy density in a thin film by the following method. We first consider the reflection and transmission of electromagnetic radiation at a thin dielectric layer between two semi-infinite media. All the media are homogeneous and isotropic. If we assume a plane wave is incident from medium 0 (glass) through medium 1 (metal) to medium 2 (air), the whole structure can be described by the indices of refraction

$$n(x) = \begin{cases} n_0, & x < 0, \\ n_1, & 0 < x < d, \\ n_2, & x > d. \end{cases} \qquad (2\text{-}21)$$

If the plane of incidence is the xz plane, the electric field vector of a plane wave solution of the wave equation can be of the form

$$\mathbf{E}(x)\exp\left[i\ (\omega t - \beta z)\right], \qquad (2\text{-}22)$$

since the medium is homogeneous in the z direction. The parameter β is the z component of the propagation wave vector. The electric field vector can be written as

$$E(x)=\begin{cases} Ae^{-ik_{0x}x} + Be^{ik_{0x}x}, & x < 0, \\ Ce^{-ik_{1x}x} + De^{ik_{1x}x}, & 0 < x < d, \\ Fe^{-ik_{2x}(x-d)}, & x > d, \end{cases} \qquad (2\text{-}23)$$

where we assume that the electric field vector is p-polarized (i.e., parallel to the plane of incidence). The complex amplitudes A, B, C, D, and F are constants, and k_{0x}, k_{1x}, and k_{2x} are the x components of the wave vectors:

$$k_{ix} = \left(\frac{\omega}{c}\right) n_i \cos\theta_i, \qquad i = 0, 1, 2, \qquad (2\text{-}24)$$

where θ_i is the ray angle measured from the x axis. The constant A is the amplitude of the incident wave. The constants B and F are amplitudes of the reflected and transmitted waves, respectively. For a p wave, the electric field **E** (x) is **z**E (x), and the y component of the magnetic field is obtained by using $H_y = -(i/\omega\mu)(\partial E/\partial x)$. Thus,

$$H_y(x)=\begin{cases} -\dfrac{k_{0x}}{\omega\mu}\left(Ae^{-ik_{0x}x} - Be^{ik_{0x}x}\right), & x < 0, \\ -\dfrac{k_{1x}}{\omega\mu}\left(Ce^{-ik_{1x}x} - De^{ik_{1x}x}\right), & 0 < x < d, \\ -\dfrac{k_{2x}}{\omega\mu}Fe^{-ik_{2x}(x-d)}, & x > d, \end{cases} \qquad (2\text{-}25)$$

where μ is the magnetic permeability constant. Imposing the continuity of E_z and H_y at the interfaces of x = 0 and x = d, we can obtain four equations. These four equations can be used to solve for B, C, D, and F in terms of A (the amplitude of incident wave). After a few steps of algebraic manipulation, and substituting the Fresnel reflection coefficient r_{12} and phase change β into the equation, we can obtain the relation between C and D as

$$D = r_{12}\, e^{-2i\beta}\, C\,. \qquad (2\text{-}26)$$

By knowing the field amplitudes, the electric field distribution in the thin films can be written as

$$E(x) = C\left(e^{-ik_{1x}x} + r_{12}e^{-2i\beta}e^{ik_{1x}x}\right), \qquad 0 < x < d. \qquad (2\text{-}27)$$

The density of the relative electromagnetic energy as a function of the distance from the medium 0 (glass) can then be evaluated by using the equation

$$U(x) = \frac{1}{2}\,\varepsilon\,|E(x)|^2\,. \qquad (2\text{-}28)$$

In Fig. 2-4, the energy densities given by Eq. (2-28) are plotted for angles near the angle of surface plasmon excitation. The reversal of field profiles at the angle of surface plasmon coupling is particularly significant since it is this feature which enhances field dependent desorption effects in our experiments.

B. MECHANISM OF DESORPTION

The absorption of laser radiation in solids can lead to laser-induced desorption. In this kind of interaction, the particles (atoms or molecules) are

released from the surface when laser energy is transferred to the surface-adsorbate bond. The effect of pulsed-laser-induced desorption depends on the laser wavelength, pulse energy, energy density, and pulse duration. Photodesorption can occur in several ways.

1. Laser-Induced Thermal Desorption (LITD).

In laser-induced thermal desorption (LITD), surface heating can result from direct lattice phonon excitation or an initial electronic excitation, e.g. *via* electron hole pairs, which subsequently decays by exciting phonons. In contrast to conventional thermal desorption, LITD may produce a large range of heating rates. At low laser irradiance, the desorption occurs with a characteristic low translational temperature (i.e. with low kinetic energy) of the desorbed species, similar to that of conventional thermal desorption. At high laser irradiance ($I > 10^9$ W/cm^2),[48] a pulsed laser can deliver high power densities in short time intervals, yielding rapid heating of small sample volumes. The rapidly delivery and large amount of heat produces shock waves[48,49] in the substrate. The recoil pressure raises the boiling point of the target above the usual vaporization temperature, and the desorbed species is ejected with high translational velocity (i. e. with high kinetic energy).

2. Vibrational Excited Desorption.

Infrared laser radiation can be coupled directly into surface vibrational modes of the system when laser frequencies match the frequencies of the lattice modes. Desorption may occur when the energy is resonantly absorbed into internal vibration modes of the

adsorbate or the adsorbate-surface vibrational modes. The desorption yield increases with the thickness of the adsorbed molecular layers. The desorption yield is generally very low, and the translational temperature is usually much lower than the peak desorption temperature observed in conventional thermal desorption. Many microscopic theories have been suggested by different scientists,[56,57,58,59,60,61] but none of them can explain the low translational temperature observed for this kind of desorption.

3. Electronic-Excited Desorption.

An ultraviolet or visible laser can induce desorption due to electronic excitation of the adsorbate-surface system. This desorption is initiated by direct photonic stimulation of a particular bond, after which desorption will occur either as a result of the disruption of the bond, or simply as a consequence of the atom being in an excited state. This is a nonthermal mechanism since the desorption is due to direct electronic excitation before the absorbed energy is transferred to lattice vibrations.

In metals, electronic-excited desorption can be induced by surface plasmon oscillations excited with photons.[37,38,39,43,50] Since there is an electromagnetic field enhancement on the surface due to surface plasmons, this excitation method provides an ideal system for the studies of electronic-excited desorption.

There are different damping (de-excitation) processes of surface plasmons on a smooth surface. In normal internal damping, the electromagnetic field of the surface plasmons excites electron-hole pairs at

the Fermi level or direct interband transitions. Since the wave vector k_z perpendicular to the surface is not fixed, a continuum of k_z is available for interaction processes, and a strong coupling of surface plasmons with the electron-hole pairs should be possible, since momentum conservation can be fulfilled. The subsequent de-excitation of the electrons and holes produces phonons and thus heat. This mechanism is properly included in simple theories through ε_2 of film and substrate. The electromagnetic field of the surface plasmons can also induce electronic excitation of localized surface modes. This extra absorption mechanism is not properly accounted for by simple theory, but it is the most likely source of laser-induced electronic-excited desorption.

There are many theories concerning laser-induced thermal desorption[51,52,53,54,55] and vibrational excited desorption, [56,57,58,59,60,61] but relatively few theories for electronically excited desorption. Available theories includes the Menzel, Gomer, and Redhead (MGR) valence excitation model,[62] the Knotek and Feibelman (KF) core-hole Auger decay model,[63] and the Z. Wu model.[64] Although the MGR and KF desorption models were originally intended for describing excitations by high energy photons (> 10 eV) and electrons, they could be quite relevant to laser-induced photodesorption.

The usual model of electron-stimulated desorption in the MGR model is that the incident beam excites a bonding electron to an antibonding or nonbonding state; as a result, the effective potential between surface atom and solid become repulsive, and the atom desorbs. A diagram illustrating the MGR model is in Fig. 2-5, where an excited electron makes a transition to

a state in which the desorbate feels the upper, purely repulsive potential. This model leaves open the question of how highly electronegative atoms such as O and F, manage to desorb as positive ions, which requires the transfer of 2 to 3 electrons.

The KF model provides an explanation of how positive ions are generated prior to desorption for ionically bonded substances. In the KF model of metal oxides, the electrons of the metal atoms are transferred to the oxygen atom. The main decay channel for a hole in the highest-lying metal-atom-core state is an interatomic Auger transition. In ionic materials, valence electrons occupy local orbitals on the electronegative atom, and an Auger transition may remove two electrons from a surface atom. The atom will then suddenly find itself in a strong repulsive Madelung well, and hence will be likely to be desorbed. In laser desorption, there is no apparent means of creating a core hole, so that this model has little direct application to the present problem.

Z. Wu described a possible mechanism that could cause ion emission below the melting point. The basic assumption in this model is that ions are emitted from surface defect sites where electronic excitation can be trapped for times comparable to the lattice relaxation time of $10^{-12} - 10^{-13}$ s. The exact nature of the defect sites is not addressed in this model.

The proposed Z. Wu mechanisms are the following:

(1) The incident laser produces an electron-hole plasma near the surface, which causes a decrease in the lattice force constant, i.e. the surface atoms become less tightly bound.

(2) Atoms at these less tightly bound surface sites desorb as ions through the so-called hole stimulated desorption (internal Auger mechanism).

(3)The crossing of ion antibonding curve and atom antibonding curve can lead to the desorption of neutrals.

CHAPTER III

EXPERIMENTAL METHODS

In this Chapter we discuss the experimental apparatus and procedures used in our experiments.

A. EXPERIMENTAL APPARATUS

The major components in this experiment are lasers and a mass spectrometer. Since lasers and mass spectrometers can be used to solve various problems,[65,66,67] we will describe the lasers, the mass spectrometer, and the data acquisition system we used in our desorption experiment in detail.

The specifications for the lasers used in this experiment are given in Table 3-1. For Nd:YAG laser, the fundamental wavelength is λ =1064 nm. The second harmonic laser light at λ = 532 nm is generated by the HG-2 harmonic generator made by the same manufacturer (Quanta-Ray) that made the Nd:YAG laser. Harmonic generation is accomplished using Type II SHG (second harmonic generator) crystals cut for the proper phase-matching angle. The output beam polarization can be conveniently rotated to any desired orientation. In the output beam, the 2nd harmonics and the fundamental, are separated by a harmonic beam splitter made by ORIEL (Model 53202). The harmonic beam splitter reflects the 1064 nm wavelength and transmits ~ 80% of the 532 nm wavelength. The 2nd

harmonic is used in our experiment and the fundamental is safely dumped into a copper cavity with nonreflecting surfaces. The 2nd harmonic beam is focused by a lens with focal length f = 50 cm, so that the spot size at the focal point is 1.2×10^{-4} cm^2. The laser fluence of the 2nd harmonic beam without attenuation is F = 140 J/cm^2 (or irradiance $I = 2.0 \times 10^{10}$ W/cm^2 since our laser pulse width is 7 ns), which is more than enough to desorb atoms from solid surfaces. The magnitude of this energy is able to produce shock waves (see Chapter II, Section B). Thus the Nd:YAG 2nd harmonic beam must be attenuated to the order of $F = 10^{-1}$ J/cm^2 (or $I = 10^6$ W/cm^2). The excimer laser beam is focused by a lens with focal length f = 25 cm, so that the spot size at the focal point is 0.06 cm x 0.15 cm. The laser fluence without attenuation is F = 8.9 J/cm^2 (or $I = 1.3 \times 10^9$ W/cm^2). The nonresonant multiphoton ionization process can be saturated by providing powers $I \geq 10^8$ W/cm^2 with these 10^{-8} sec pulses.[68,69]

The time-of-flight mass spectrometer (TOF-MS) consists of four major parts; acceleration plates, deflection plates,a free flight tube, and an electron multiplier. A schematic of the TOF-MS system is shown in Fig. 3-1. Plates 1,2,and 3 are the acceleration plates. The plate 1 is held at 1600 V, the plate 2 is at 1300 V, and the plate 3 is grounded. The plate 2 has a 0.6 cm diameter hole and the plate 3 has a 2.5 cm diameter hole at the center covered with 85% transparent nickel mesh. The deflection plates, which are labeled by number 4 in Fig. 3-1, consist of two orthogonal pairs. Deflection plates are used to center the beam on the detector. However, if the acceleration plates are indeed flat, orthogonal to the flight tube axis, and the accelerated ion beam has a translational energy less than 1 eV, the

deflection plates can usually be turned off during operation. In the field-free drift tube (5 in Fig. 3-1), the ions separate in time according to the square root of the mass-to-charge ratio ($\sqrt{m/e}$) by virtue of their different velocities. The lighter bunches speed ahead while the heavier ions lag behind. The electron multiplier (6 in Fig. 3-1), is a THORN EMI-Gencom Model 9603/2, which has BeCu secondary emitting surfaces, gain of 5×10^5 at normal operation potential of – 2.5 kV, and detection efficiencies of 85% are obtained for ions of impact energy ≥ 18 keV. The spacings in the TOF-MS are indicated in the Fig. 3-1. These dimensions are fixed, but the voltages for the three plates that define the source and accelerating regions are determined by the requirement for optimum spatial resolution.[70]

The data acquisition system is a LeCroy Century Model 2002 transient digitizing system, which includes two Model TR8828C waveform digitizers, two Model MM8104 sample memories, a Model 6103 dual channel amplifier/trigger generator, and a Model 8901A GPIB instrument interface. All of these are fitted into the LeCroy Model 8013A benchtop instrument mainframe. The 2002 provides a maximum digitizing rate 200 MS/sec (megasample per second; sample interval 5 nsec), a 32K sample per channel memory, and input signal conditioning from 50 mV to 50 V fullscale. When the signal of interest is short compared to the duration of one repetition, the hardware cost per event is high because of the long memory required. The TR8828C BURST MODE feature allows the user to record only the signals of interest into memory and to block out or disregard the non-important dead time between events. Thus the system has deep memories for uninterrupted recording of high frequency signals without

reducing the sample rate. The system is controlled by a NCR-PC (80286 with mathematics coprocessor) running WAVEFORM-CATALYST-PLUS software (LeCroy Model 6900). The NCR-PC has a color terminal, a 20 Mb internal hard disk, and two 5 1/2 inch floppy disk drives. A printer (EPSON LX-800), which can print out the mass spectrum signals, is connected to the NCR-PC.

The rest of the electronic components used in this experiment are listed in Table 3-2. The amplifier must be linear and must preserve the shape of mass spectrum signals with risetimes and falltimes less than 10 ns. The fast amplifier (LeCroy 612AM) is a six channel variable amplifier. We use this to amplify the signal from the electron multiplier and the signal from the photodiode. The linear fan-in fan-out (LeCroy 428F) is a quadruple input and output amplifier, which can sum four input signals to one output signal or can fan out one input signal to four output signals without any distortion. The signals from the electron multiplier are also directed to two oscilloscopes. One oscilloscope (HP 1744A) is triggered by the Nd:YAG laser and is used for monitoring the delay time and plasma production. Another oscilloscope is triggered by a photodiode (firing from the excimer laser) and is used for monitoring the desorption signals.

B. EXPERIMENTAL PROCEDURES

The dimensions of the right angle glass (BK-7) prism is 1.0 cm x 1.0 cm x 1.0 cm. Al films can be removed from prisms by diluted NaOH, Ag films

by diluted nitric acid, and Au films by a solution consisting of 3 parts HCl acid, 1 part nitric acid, and 4 parts water. Rhodamine B films can be dissolved in methyl alcohol. The prism is washed with microwash and deionized water, then washed with acetone and methyl alcohol in an ultrasonic cleaner. The thin films are deposited on the prism in a vacuum evaporator with a base pressure of 10^{-6} Torr. The film thickness is measured by a quartz-crystal thickness monitor (for a known material's density, various thicknesses can be obtained by a change in the vibration frequency of the crystal). The Al films are prepared by evaporating 99.999% aluminum wire that is wrapped around a tungsten wire. The thickness of the Al film in this experiment is 27 ± 1 nm. The Au films are prepared by evaporating 24 K gold wire that is placed in a tungsten boat. The thickness of the gold films in this experiment is 38 ± 1 nm. The Ag films are made by evaporating silver powder from a tungsten boat. The thickness of the silver films in this experiment is 38 ± 1 nm. The rhodamine B films are prepared by evaporating rhodamine B powder (laser grade high purity dye made by Exciton,Inc.) in a tungsten boat by slow heating at a very low temperature ($< 200^{\circ}$ C). The thickness of the rhodamine B film is 80 nm.

The laser power is measured by a laser power meter made by Scientech (Model 362). Since the beam size is known, we can calculate the fluence and the irradiance. The Nd:YAG laser beam is attenuated by a set of glass slides. The reflection of each surface provides approximately a 4% decrease of the laser intensity. By varying the number of slides, we can obtain the proper laser intensity. The laser power is measured after the beam passes through the attenuation slides, but before the focusing lens,

window, and prism surface (because the laser power meter can not be fitted into the vacuum chamber or the space between the chamber and the lens). Thus in the calculation for laser fluence at the thin film surface, we subtracted losses for those surfaces which are located downstream from the laser power meter. The reflection of all surfaces (except the prism surface) has been calibrated in air, and the result is in agreement with the calculation.

The experimental arrangement for laser desorption is shown in Fig. 3-2. Since we need a p-polarized beam with vertical electric field vector to induce surface plasmons, the beam path has to be horizontal. This can be checked by rotating each mirror perpendicular to the incident beam to see if the reflected beam is superimposed on the incident beam. The scanning mirror M_r is calibrated using the same method. If M_r is at 45 degree, the reflected beam from the prism surface should be superimposed to the incident beam on the mirror surface.

The desorption experiments are performed in a cryopumped vacuum system with a base pressure of 10^{-7} Torr. The metal-coated prism is placed in the corner of the acceleration plates (see Fig. 3-2) of the time-of-flight mass spectrometer (TOF-MS). The flight path of the ions in the TOF-MS is perpendicular to the plane of the figure. P-polarized light from the second harmonic of a Nd:YAG laser with wavelength 532 nm and pulse length 7 ns is passed through the prism onto the sample. The angle of incidence can be fine tuned by rotating the mirror M_r, as illustrated in Fig. 3-3. This rotation moves the laser beam to a fresh spot on the prism surface at each different angle of incidence. Desorbed neutral atoms are ionized over the entrance

aperture of the TOF-MS by an XeCl excimer laser with a wavelength of 308 nm and a pulse length of 7 ns. The ions are detected by an electron multiplier in the TOF-MS.

The electronics used in the desorption experiment are shown schematically in Fig. 3-4. The triggering device of the Nd:YAG laser is connected to a delay generator which, after a chosen time delay, will trigger the excimer laser. By varying the delay time between the two lasers, we are able to determine the kinetic energy of the desorbed neutrals. The Nd:YAG laser is set at a repetition rate of 10 Hz. Part of the light from the excimer laser is monitored by a photo-diode which triggers the transient digitizer. The ion signal from the TOF-MS is amplified by a fast amplifier and recorded by the transient digitizer. The transient digitizer is run by a PC-AT compatible computer with mathematic coprocessor. The desorption yield in this experiment is the integrated yield produced by 100 laser pulses at the same angle and excitation spot, calculated on-line by the PC-AT during the experiment.

CHAPTER IV

RESULTS AND COMPARISONS

A. DESORPTION OF METAL FILMS

We have observed that the three metals Al, Au, and Ag can all be efficiently desorbed from the prism at angles near the plasmon resonance. Since we detect very few ions in this process, particles desorbed from surface are mostly neutral . These data are presented below for each metal.

1. Aluminum Film

The desorption yield of Al atoms from the Al film at various angles of incidence near the surface plasmon resonance is given in Fig. 4-1. Curves A-1 and A-2 are the desorption yields observed with the laser beam incident through the prism in the geometry required to excite surface plasmons. The curves show sharp peaks, which we associate with plasmon excitation, near the angle $\theta = 43^{o}$. For curve A-2, the laser power level was 0.43 ± 0.01 mJ/pulse, as measured by a laser power/energy meter. We estimate a fluence (F) on the film of 210 ± 5 mJ/cm^2. For A-1, the fluence is 15% less, and the ion yield also becomes 15% smaller. Curves B-1 and B-2 of Fig. 4-1 exhibit the desorption yield obtained with the same sample, and the same angles and power levels, but with illumination from the front surface, rather than through the prism. These data show yields produced at the same power levels but without the excitation of surface plasmon. A small, essentially uniform yield of Al atoms is

observed at all incident angles. The desorption yields for this geometry are observed to increase nonlinearly with F.

In Fig. 4-2, we show the energy absorbed by the Al film (A), calculated by using Eq. (2-4), Eq. (2-5), and Eq. (2-6) with Al film thickness d = 27 ± 1 nm, and the index of refraction $n_0 = 1.5$, $n_1 = 0.70 + i\,5.12$,[71] $n_2 = 1$. Good agreement is seen between the total absorption A and the desorption yield (curve A-1) in Fig. 4-2. Similar agreement is found for curve A-2 (not shown). The almost identical dependence of the desorption yield and the absorption on incidence angle provides strong evidence that the desorption yield of the Al atoms depends linearly on the energy absorbed by the film. We have also measured the yield at the plasmon resonance peak as a function of laser fluence, and observed that the desorption yield depends linearly on the laser fluence in the range from about 100 mJ/cm^2 up to 500 mJ/cm^2. The dependence of the desorption yield at the plasmon resonant angle on the laser power is displayed in Fig. 4-3. There is a linear dependence on power above a threshold of about 2 mW. For laser fluence above 500 ± 20 mJ/cm^2, significant desorption is observed at all angles.

Varying the time delay between the desorbing Nd:YAG laser and the ionizing excimer laser allows us to measure arrival time distributions of the desorbed species. The timing sequence for this kind of measurement needs some description. After the desorbing laser has been fired at the target, bursts of neutral atoms emitted by the target pass through the ionization region just above the

extraction aperture in the middle between the acceleration plates of the TOF-MS. These desorbed particles have different translational velocities, so that the fast ones reach the ionization region earlier than the slow ones. Pulses from the ionizing laser arrive after a variable delay (0-200 μs) and are focused through the ionization region. Thus at various delay times, particles with various velocities are ionized.

The delay time distribution of desorbed Al atoms was obtained by measuring ion yield as a function of delay time. Since the distance from the surface to the ionization region was known, we could transform the delay time distribution to a velocity distribution and kinetic energy distribution by a simple calculation.[72] The kinetic energy distributions derived from these value are shown in Fig. 4-4. There are two peaks, one at 0.081 eV, and another at 0.50 eV. The slow peak is due to a thermal effect and corresponds to a translational temperature of approximately 9.0×10^2 °K (given by T = K.E./k, where k is the Boltzmann constant). The estimated error in the kinetic energy and the temperature are 10% and are mainly due to uncertainty in the time-of-flight measurement. The peak at 0.081 eV moves to higher energy as the laser fluence increases. The 0.50 eV peak position does not vary with the changing of laser fluence within the range from 100mJ/cm^2 to 500 mJ/cm^2.

We repeated the desorption experiment with the same experimental condition but with a s-polarized laser beam. We did

not observed any desorption signal within the range of laser fluence from 100 mJ/cm^2 to 500 mJ/cm^2.

The result cited above are given in arbitrary units and thus provide information about relative desorption rates only. We have obtained a rough estimate of the absolute number of desorbed atoms/incident photon at the absorption maximum at the plasmon resonance angle. For the 27 nm Al film, desorption was continued until all Al was removed from the 0.1 mm^2 area of the incident beam. We find a desorption of (0.2 – 1) x 10^{-6} ions/photon where the lower estimate is provided by calculating the average loss per pulse and the upper estimate by the extrapolated value for the desorption in the first few pulses. This value is comparable to the value of 7.1 x 10^{-6} cited by W. Hoheisel[37] in his studies of plasmon-coupled desorption on rough surfaces.

2. Gold Film

The desorption yield of Au atoms from the Au film at various angles of incidence is given in Fig. 4-5. The thickness of the Au film on the prism is 38 nm, and the optical constant is $n_1 = 0.47 + i\,2.41$. We use the same equations to calculate the optical absorption as we did in Al film. The result shows good agreement between the desorption yield and energy absorbed by the Au film. This demonstrates that the desorption yield of Au atoms, like that of Al, depends linearly on the energy absorbed by the Au film. There is a fluence threshold at about 100 mJ/cm^2 , below which the signal cannot be distinguished from the noise.

The kinetic energy (KE) distribution for Au atoms desorbed from the Au film is given in Fig. 4-6. There are two peaks, one at about 0.082 eV, and another one at about 0.33 eV. The slow peak corresponds to a temperature about 9.0×10^2 °K, and is a thermal peak. The delay time distribution for the slow peak at different laser fluence, is shown in Fig. 4-7. At F = 300 mJ/cm^2, the peak is at 57 μs, which correspond to KE = 0.094 eV. At F = 500 mJ/cm^2, the peak is at 46 μs, which correspond to KE = 0.14 eV. The temperature variation of the thermal peak with laser fluence is shown in Fig. 4-8. The estimated error in the kinetic temperature is 10%. The position of the slow peak moves to higher energy (or higher temperature, eV/k, as shown in Fig. 4-8), as the laser fluence increases. The position of the high energy peak at 0.33eV does not vary with the laser fluence.

3. Silver Film

The desorption yield of Ag atoms from the Ag film at various incident angles is given in Fig. 4-9. The optical absorption is obtained by the same method as Al and Au, but with different optical constants $n_1 = 0.13 + i\,3.12$. The thickness of the Ag film on the prism is 38 nm. The comparison between the Ag desorption yield and the energy absorption shows good agreement. This shows that the desorption yield of Ag atoms depends linearly on the energy absorbed by the Ag film. The threshold for the desorption signal is observed at the laser fluence of about F = 100 mJ/cm^2.

The kinetic energy (KE) distribution for the desorbed Ag atoms is demonstrated in Fig. 4-10. The position of the fast peak is at 0.90 eV. The position of the slow peak is at about 0.081 eV which corresponds to a thermal temperature of about 9.0×10^2 °K. Since the translational kinetic energy of the 0.90 eV peak is very close to the detection limit ($\approx$ 0.1 eV, see Chapter III, Section A) of our mass spectrometer, we turned on our deflection plates and repeated our experiment to be sure that we were not measuring the low energy tail of a higher energy peak. We applied a voltage of 3 eV to the deflection plates which would enable us to detect ions with KE up to 4 eV. We did not detect any particle with KE higher than 1 eV, but were still able to detect the 0.90 eV peak with slightly reduced intensity. The 0.081 eV peak cannot be detected when the deflection plates are on.

The desorption results for Al, Au, and Ag are very similar. The major features may be summarized as follows:

(1) For each metal, the desorption yield follows closely the absorption curve. This implies a linear dependence of desorption on the number of photons absorbed. This linear dependence of yield on photon flux was also observed for Al by measuring the peak yield as a function of laser intensity.

(2) For each metal, the kinetic energy distribution of desorbed atoms show two peaks, one near 0.08 eV (900° K) that is nearly the same for each material, and a second high energy peak of variable energy.

(3) The high energy peaks in the kinetic distribution for Al, Au, and Ag are observed at 0.50, 0.33, and 0.90 eV, respectively. The significance of these values will be discussed further in the following Chapter of this dissertation. (4) We also observed peaks in the mass spectra from Si and SiO_2 in the prism. Both of them have a low energy peak near 0.08 eV, but do not have the high energy peak. The observation of Si and SiO_2 in the mass spectra led us to examine the question of whether energy was absorbed at the prism-film or film-vacuum interfaces. Which interface absorption induces the desorption in this experiment ? This question will be discussed in the following Chapter.

B.DESORPTION OF RHODAMINE B

In samples with rhodamine B adsorbed on an Al film, we found that at the plasmon resonance angle there were two peaks in the mass spectrum, corresponding to the masses of Al and of the rhodamine B molecule. Rhodamine B is a large molecule with molecular weight 479 amu, ionization potential 6.7 eV,[73] absorption maximum 540 nm, and the molecular structure shown in Fig. 4-11. We choose the rhodamine B as our sample because its optical and electronic properties are well known, it is a large molecule, and it dissociates at 200 °C which is relatively low compared with the observed temperature of those metal we have desorbed. The important implication of this result is that the large and fragile rhodamine B molecule can be efficiently desorbed by this method without fragmentation.

Fig. 4-12 and Fig. 4-13 display the desorption yield of both Al and rhodamine B at various laser incident angle. Both signals showed a dependence with incident angle, which peaked at the plasmon resonance angle. The laser fluence in Fig. 4-12 is F = 210 ± 5 mJ/cm^2 and the laser fluence in Fig. 4-13 is F = 178 ± 5 mJ/cm^2.

The number of fragment ions of rhodamine B were at least an order of magnitude weaker than the number of complete molecular ions and were very close to the background noise. The threshold for both Al and rhodamine desorption signals was observed at a laser fluence of about F = 80 mJ/cm^2. Rhodamine B has only one peak at KE = 0.56 eV. Rhodamine's thermal peak was not observed due to the fragile nature of the molecule. At laser fluence exceeding about F = 300 mJ/cm^2 the mass spectrum signal of rhodamine B disappeared and significant fragmentation signals appeared. The maximum rhodamine B desorption yield at the plasmon resonance angle was obtained at the laser fluence F = 178 ± 5 mJ/cm^2. When the fluence exceeded F = 178 ± 5 mJ/cm^2, the magnitude of rhodamine B peak decreased but the magnitude of Al peak increased. When the laser fluence was above F = 500 mJ/cm^2, the Al peak broadened in both directions of the incident angle and significant desorption of Al was observed at all angles.

After several experimental runs an observable deposit of rhodamine B appeared at the edges of the aperture in the time-of-flight acceleration plates. This provided further evidence that this method removed rhodamine B intact from the Al surface.

We have also deposited the same rhodamine B film on top of a glass slide substrate and pointed the laser beam directly on the rhodamine B film.

The desorption of rhodamine B was not observed for laser fluences up to F = 500 mJ/cm^2.

CHAPTER V

DISCUSSION AND CONCLUSION

A. SUMMARY OF RESULTS

Surface plasmons excited by a second harmonic Nd:YAG laser beam in an attenuated-total-reflection (ATR) geometry were used to desorb Al, Au, and Ag atoms, and rhodamine B molecules from smooth thin film surfaces. The desorbed neutrals were ionized by a XeCl excimer laser. The desorption yields were detected by a time-of-flight mass spectrometer (TOF-MS), and recorded by an AT-PC based data acquisition system.

The desorption yield was found to be linear with energy deposition. This is confirmed by varying both the optical absorption and the laser fluence. The optical absorption varies by more than an order of magnitude with incidence angle in the ATR configuration. The laser fluence can be changed by attenuating the beam intensity.

Desorption is observed only above a threshold for the Nd:YAG laser fluence. The laser fluence was monitored by measuring the laser power with a power meter, and then was calculated by considering all the factors which include laser beam divergence, repetition rate, the focus of the lens, and the reflectances of all the surfaces. The value of the threshold is estimated to be $F = 80\ mJ/cm^2$.

We have evaluated the kinetic energy distributions of Al, Au, Ag, Si, and SiO_2 desorbed in this experiment. The Al, Au, and Ag are desorbed

from the thin film. The Si atoms, and SiO_2 molecules are ejected from the prism. The kinetic energy distribution is calculated from the translational velocity distribution. By varying the delay time between the Nd:YAG laser and XeCl excimer laser, we are able to obtain the translational velocity distribution. There are two peaks in Al, Au, and Ag kinetic energy distributions. The low energy thermal peaks for all three metals have the same value of about 0.08 eV, and move to higher energy as the laser intensity increases. The high energy peak has a different value for each metal. These kinetic energies are four to eleven times higher than the kinetic energy of the respective thermal peak (Al : 6, Au : 4, and Ag : 11). The position of the high energy peak is independent of the laser intensity. There is only one peak in the Si and SiO_2 kinetic energy distribution. This is a low energy thermal peak with the same value of about 0.08 eV, and varies slightly with laser intensity. We have listed the kinetic energies of all the desorbed particles in Table 5-1.

The most interesting observation from a practical perspective was the desorption of large rhodamine B molecules from an Al film without significant fragmentation at the plasmon resonance angle. The threshold for observing the desorption is 80 mJ/cm^2 (0.008 GW/cm^2) . Compared with previous work done by S.V. Chekalin *et al.* (for detail, see Chapter I , Section B), the magnitude of our threshold was 30 times smaller. This is due to the surface plasmon's amplification effect of electromagnetic energy density on the metal / rhodamine interface. The maximum desorption yield of rhodamine B was obtained at F = 178 ± 5 mJ/cm^2. The Al peak was observed in the mass spectrum along with the rhodamine peak. Both species have the same laser

fluence threshold. Since Al atoms of the substrate film are always observed along with the rhodamine molecules, it indicates that Al desorption is a large area excitation. This is also evidenced by physical damage observable on the metal film.

It has been shown previously that neutral desorbed species (such as large organic molecules) can be ionized by an ultraviolet laser without fragmentation and this process is called soft ionization.[74] Thus a nonthermal desorption technique becomes very important if we want to utilize the advantage of the soft ionization and resonance ionization. Techniques for desorption without fragmentation are required for quality control monitoring in the pharmaceutical industry and for unique identification in pharmacological and clinical analysis.[75] In order to use these techniques on a solid sample directly, the laser desorption has to be nonthermal. Desorption induced by surface plasmons in an attenuated-total-reflection (ATR) geometry has the potential to become a versatile means of producing nonthermal desorption of large organic molecules.

B. DISCUSSION

Since we have observed two peaks in the kinetic energy distribution of Al, Au, and Ag, one low energy thermal peak and one high energy peak, it is very important to identify the desorption mechanism for the high energy peak. There are several desorption mechanisms which have been mentioned in Chapter II, Section C. One can identify different desorption

mechanisms by analyzing the different characteristics of the desorption yield.

We can compare our experimental results with the characteristics of the different desorption mechanism as follows.

1. Laser-Induced Thermal Desorption (LITD).

Thermal desorption varies exponentially with temperature, and the temperature varies linearly with the laser energy (I_0) deposited in the material. Thus the desorption yield is not linearly dependent upon the energy deposition in the material. The desorption rate we observed depends linearly on the energy deposition in the sample. Also in thermal desorption, the kinetic energy of the desorbed neutral should increase as the energy deposition on the sample increases. In our experiment, the position of the high energy peak does not change as the energy deposition changes. These results indicate that the desorption mechanism is non-thermal.

In order to produce shock waves, the laser irradiance usually has to be above the order of 10^9 W/cm^2.[76] The laser irradiance we used here is on the order of 10^6 W/cm^2. Due to the interaction of the surface with the blowoff material, the different desorbed neutrals produced by shock waves should have the same momentum, which depends upon the laser intensity. Neuman[77] measured the momentum for Cu, Al, steel, brass, and Ta irradiated with a 0.3 J, 50 ns laser pulse, and found that the value of the momentum varied very little for different materials and was approximately 0.18 dyn sec. In our experiment, metal and substrate atoms do not have the same

momentum (TABLE 5-1). We conclude that the high energy neutrals are not induced by shock waves.

2. Vibrational-Excited Desorption.

The energies involved in vibrational-excited desorption are associated with the infrared region of the spectrum. The laser energy we use in this experiment is in the visible region (532 nm). The kinetic energy of the desorbed neutrals from vibrational-excited desorption is usually much lower than that observed in thermal desorption. In our experiment, the kinetic energy observed is much higher than in thermal desorption. We can therefore rule out vibrational-excited desorption as the mechanism for the high energy peak.

3. Electronic-Excited Desorption.

In electronic-excited desorption, at a given coverage, the desorption yield increases linearly with fluence until the thermal effect takes over. Also the peak positions and the shapes of TOF signals remain the same for different laser fluence. These characteristics in our data indicate that the desorption mechanism in our experiment is electronic-excited desorption. It is possible that the final state of the electronic transition is vibrationally excited as in the well produced by Franck-Condon excitation.

Since desorption of Si and SiO_2 is also detected, we examined the possibility that desorption was associated with energy absorption at the substrate-film interface rather than within the film. By using Eq. (2-14), we can calculate the electromagnetic energy density profile inside the thin film.

The electromagnetic energy density as a function of distance from the glass prism (ε_0), is plotted for Al, Au, and Ag, in Fig. 5-1, Fig. 5-2, and Fig. 5-3, respectively. The spatial variation of the field intensity in resonance and out of resonance are demonstrated. Surface waves at both interfaces show an exponential decay. At the resonant angle there is an electromagnetic field enhancement on the film-vacuum interface; the field density there is much larger than the field density at the prism-film interface. This indicates that the electronic energy deposition leading to desorption is most likely to take place at the film-vacuum interface. The lack of a high energy peak for Si and SiO_2, also indicates that the electronic excitation takes place at the film-vacuum interface.

We can compare the desorption yield with both the total optical absorption in the film and with the electromagnetic energy density on the surface at the film-vacuum interface. The optical absorption of a thin film at different incident angles can be obtained from Eq. (2-6). Alternatively, at a given distance $x = d$, we can use Eq. (2-14) to evaluate the density of electromagnetic energy at the film-vacuum interface. In Fig. 5-4, 5-5,and 5-6, we compare the desorption yield with the total absorption (dashed line) and with the energy density at the film-vacuum interface, and find that the yield agrees better with the surface intensity plot. This is particularly true at angles just below the plasmon angle where both the yield and surface intensity go to near zero. In this region most of the residual absorption occurs at the substrate-film interface and does not effectively contribute to the desorption yield. These results show that indeed electronic-excited desorption occurs at the film-vacuum interface.

Our desorption mechanism is better described by Z. Wu (see Chapter II, Section B). The basic assumption used by Z. Wu is that the electronic excitation can be trapped in surface defect sites in a metal. Also on a real surface, adsorption and desorption are frequently completely controlled by surface defects.[78,79] Rendulic[80] observed a shift of a hydrogen desorption peak towards lower temperatures by about 50 ^{o}K from a moderately defective (surface defect concentration < 5%) Ni surface. The influence of foreign atoms is similar to defects which reduce the sticking coefficient. Thus the desorption induced by defect-trapped electronic excitation needs less desorption energy to break the bond. In our experiment, surface plasmons may produce electron-hole pairs near surface defects, which would lead to a decrease in the lattice force constant. Particles at these less tightly bound regions might then desorb as ions through Auger decay. The crossing of the ion antibonding curve and atom antibonding curve could then lead to the desorption of neutrals. This model can be tested by further experiments, such as epitaxial growth of a metal film with controlled surface defects (steps, point defects, and impurities of foreign atoms) on a single crystal so we can examine defect related desorption closely.

We have shown that the desorption in our experiment is neither laser-induced thermal desorption nor vibrational-excited desorption. Our experimental results indicate that the desorption is electronic-excited desorption. We have also shown that the desorption was associated with energy absorption at the film-vacuum interface rather than the substrate-film interface. The desorption yield agrees better with the energy absorption at the film-vacuum interface than the total absorption in the film. It is therefore

concluded that the plasma oscillation is not necessarily damped by coupling to the phonon modes, but that a different de-excitation channel exists. Since evidence exists for electronic-excited desorption, the deexcitation channel appears to induce bond rupture of the metal overlayer.

APPENDIX

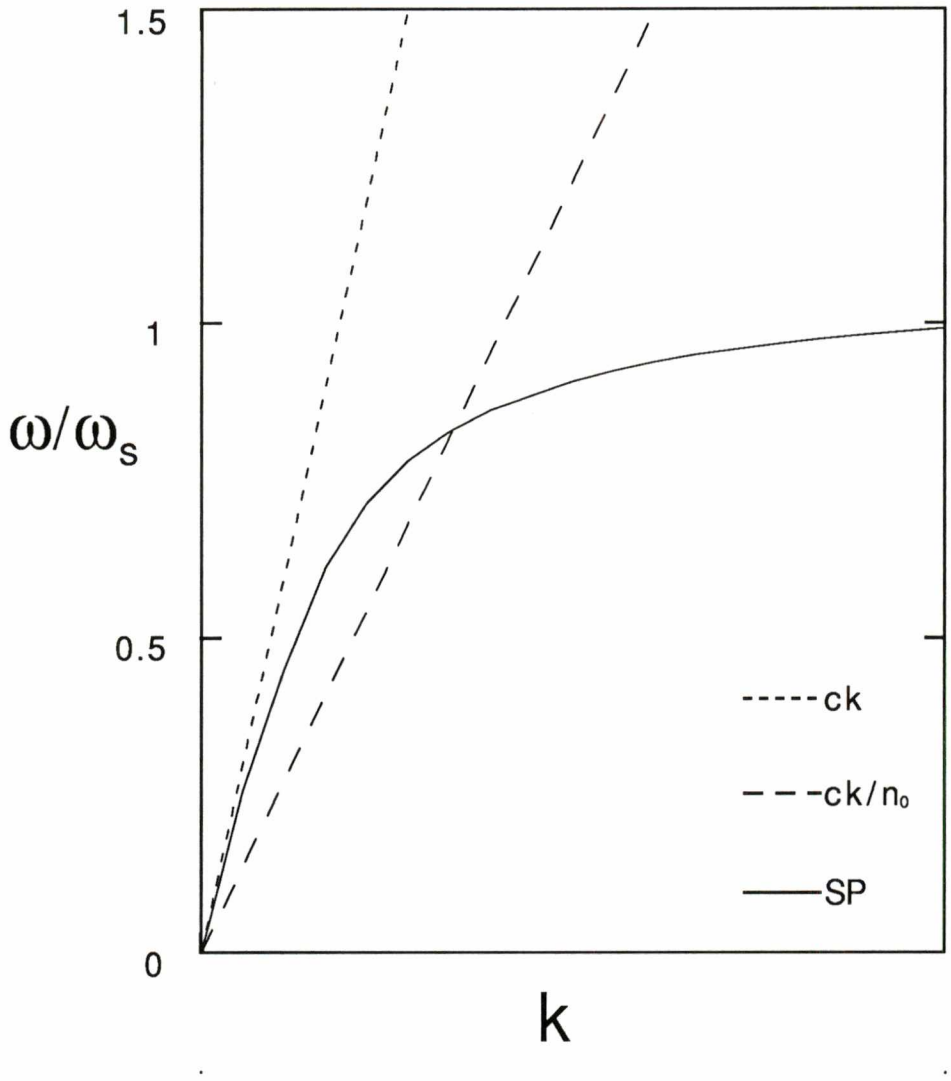

Fig. 2-1. Surface plasmon dispersion relation (SP) for a free-electron metal. The line ck is the light line in vacuum and ck/n_0 is the light line in a dielectric.

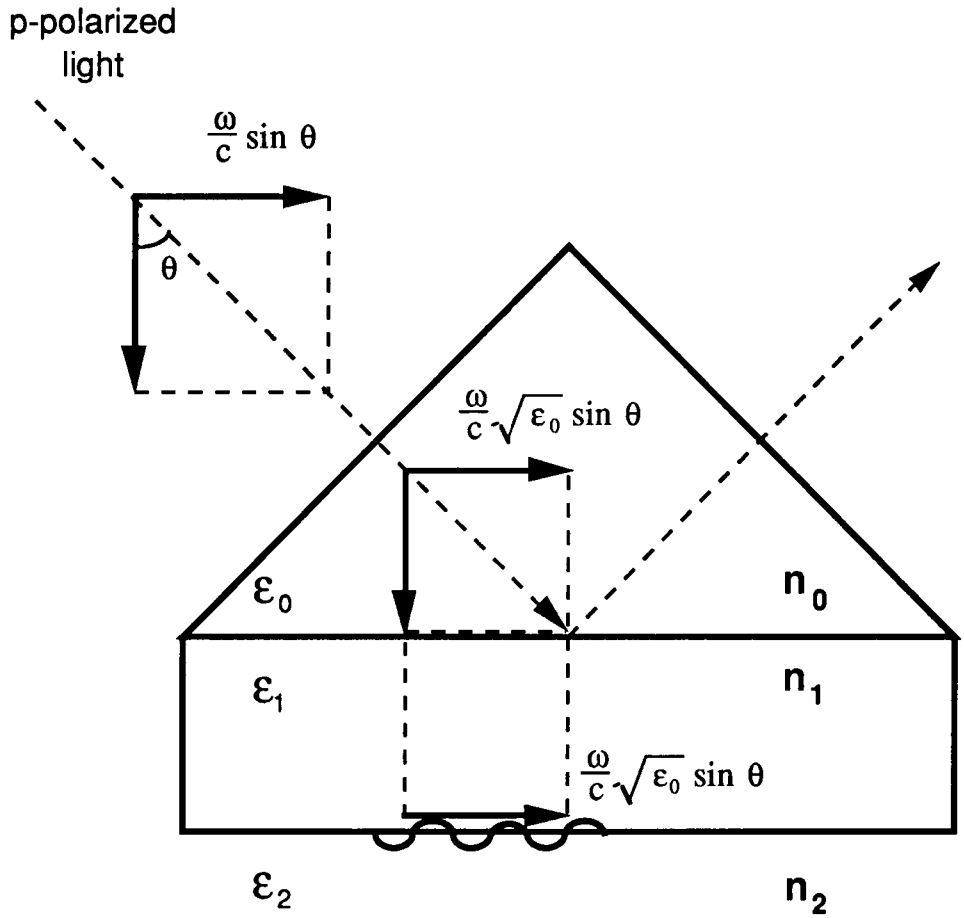

Fig. 2-2. Principle of the optical excitation of surface plasmons by attenuated total reflection (ATR) in the Kretschmann configuration.

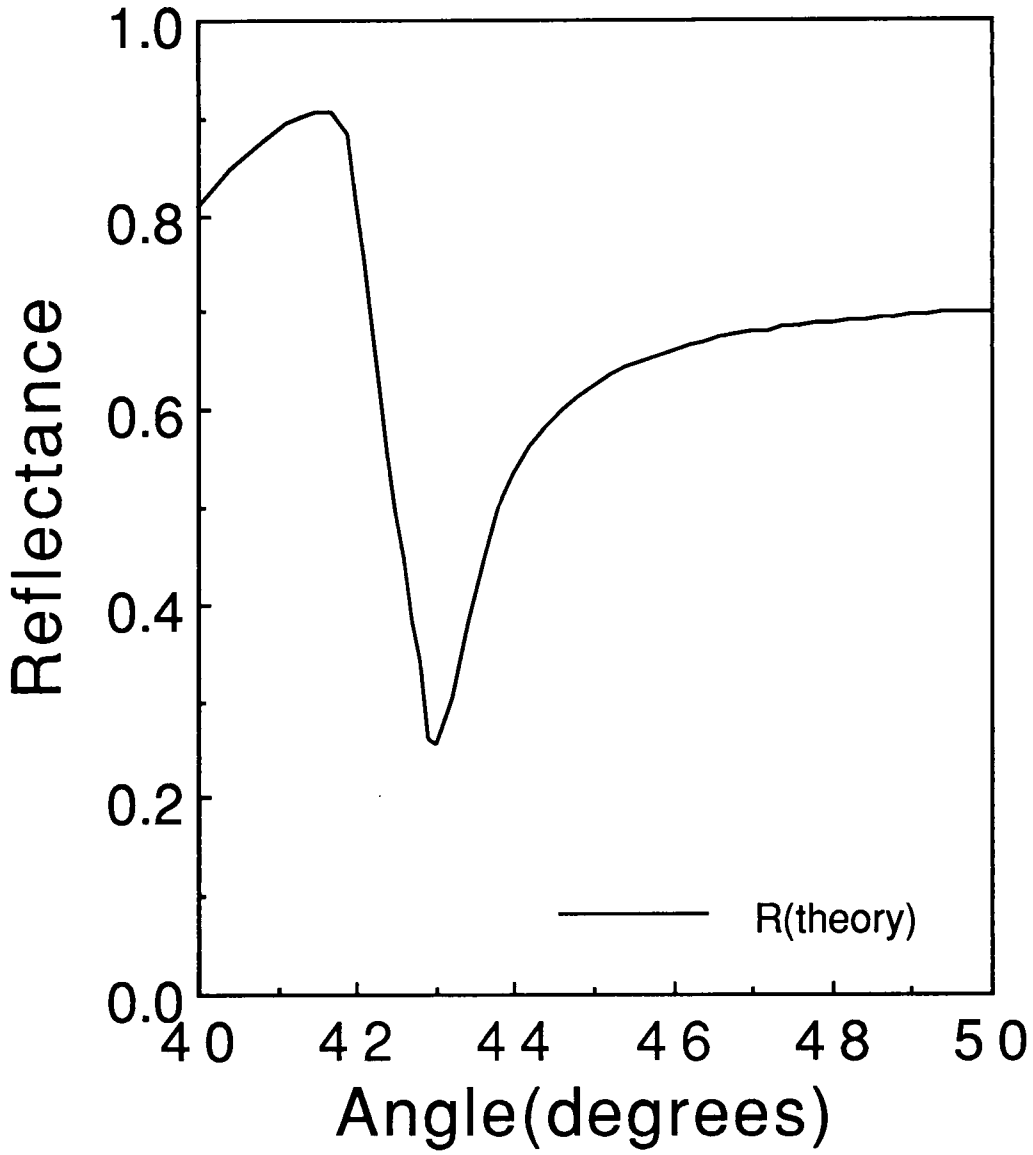

Fig. 2-3. Reflectance R as a function of incidence angle. Note that R drops sharply at the plasmon resonance angle.

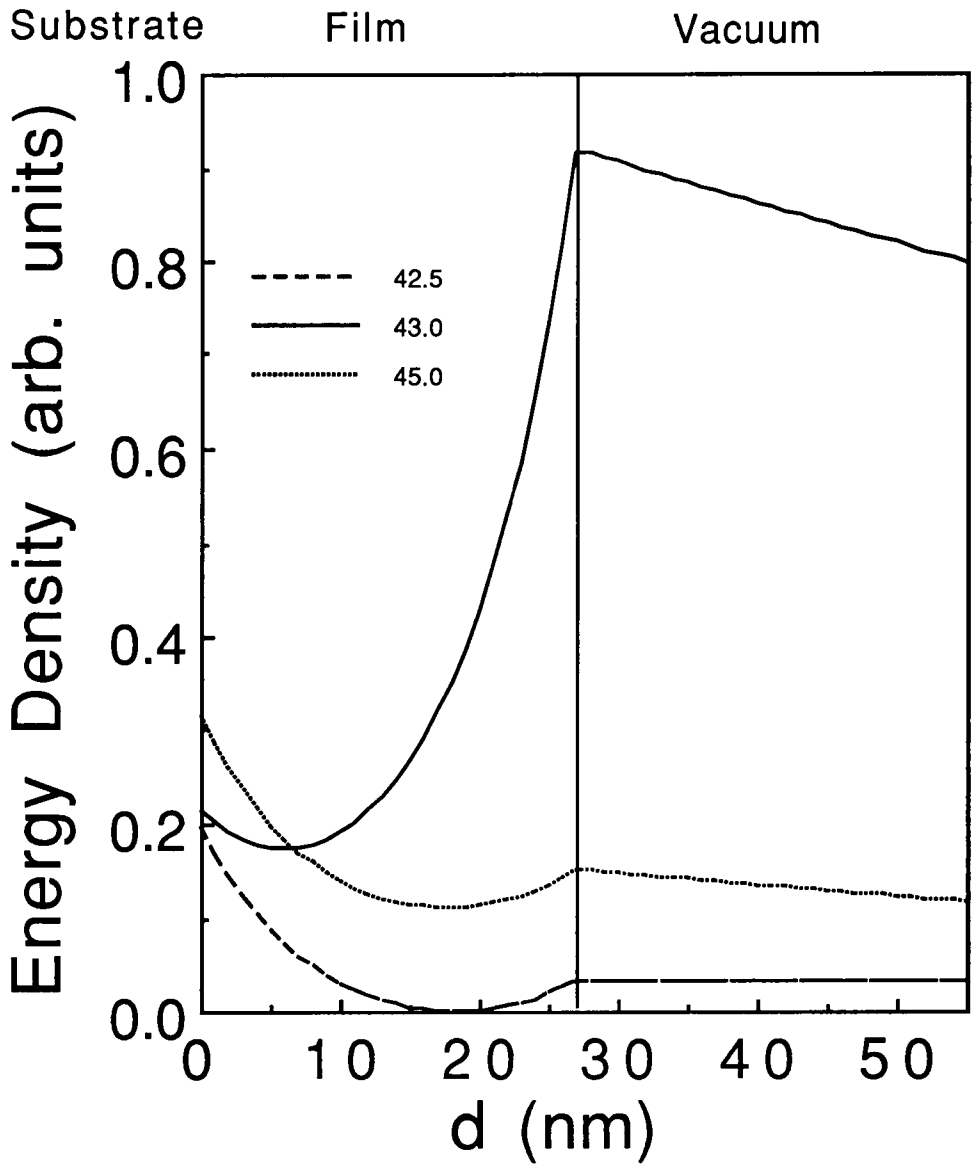

Fig. 2-4. Energy densities of the electromagnetic field from laser light at different incidence angles. We assume the substrate is glass, wavelength is 532 nm, and the film is Al. The plasmon resonance angle in this case is 43°.

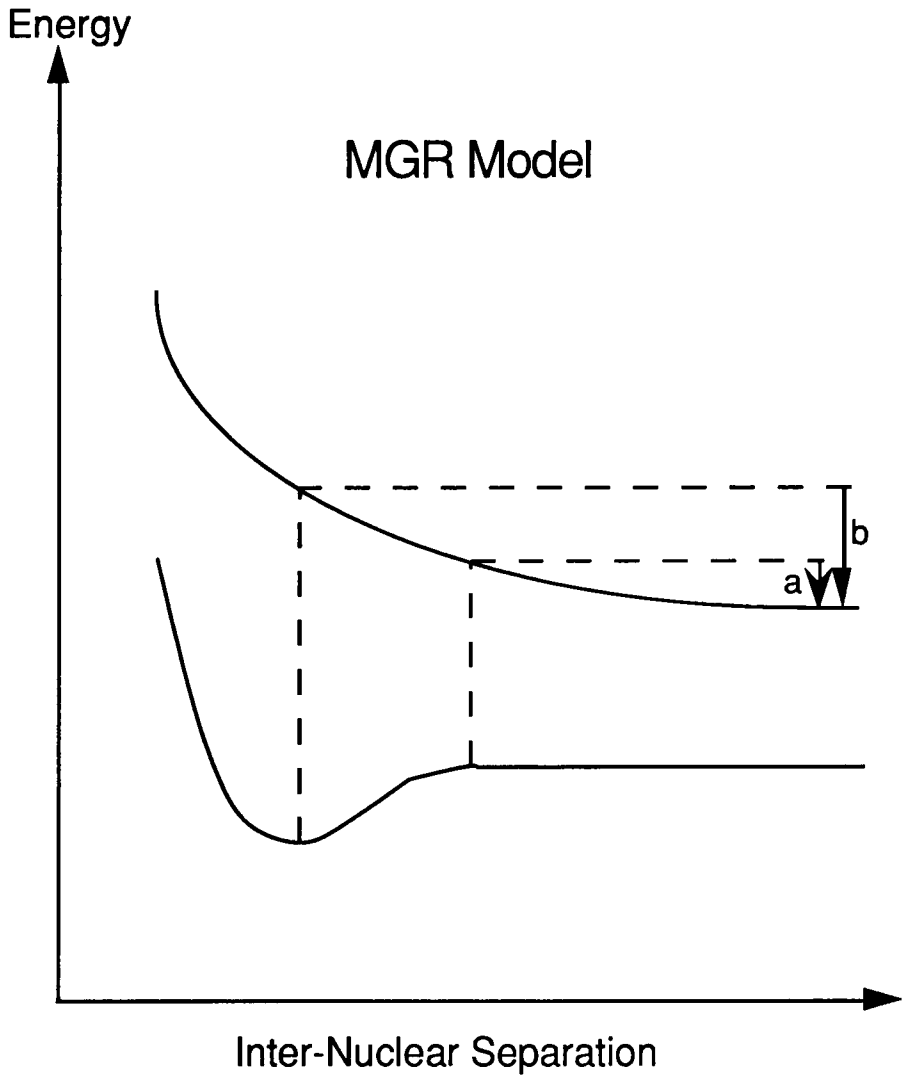

Fig. 2-5. Menzel,Gomer, and Redhead (MGR) model of electronic-excited desorption. Note that a is the minimum observable K.E. and b is K.E. of desorbing particle.

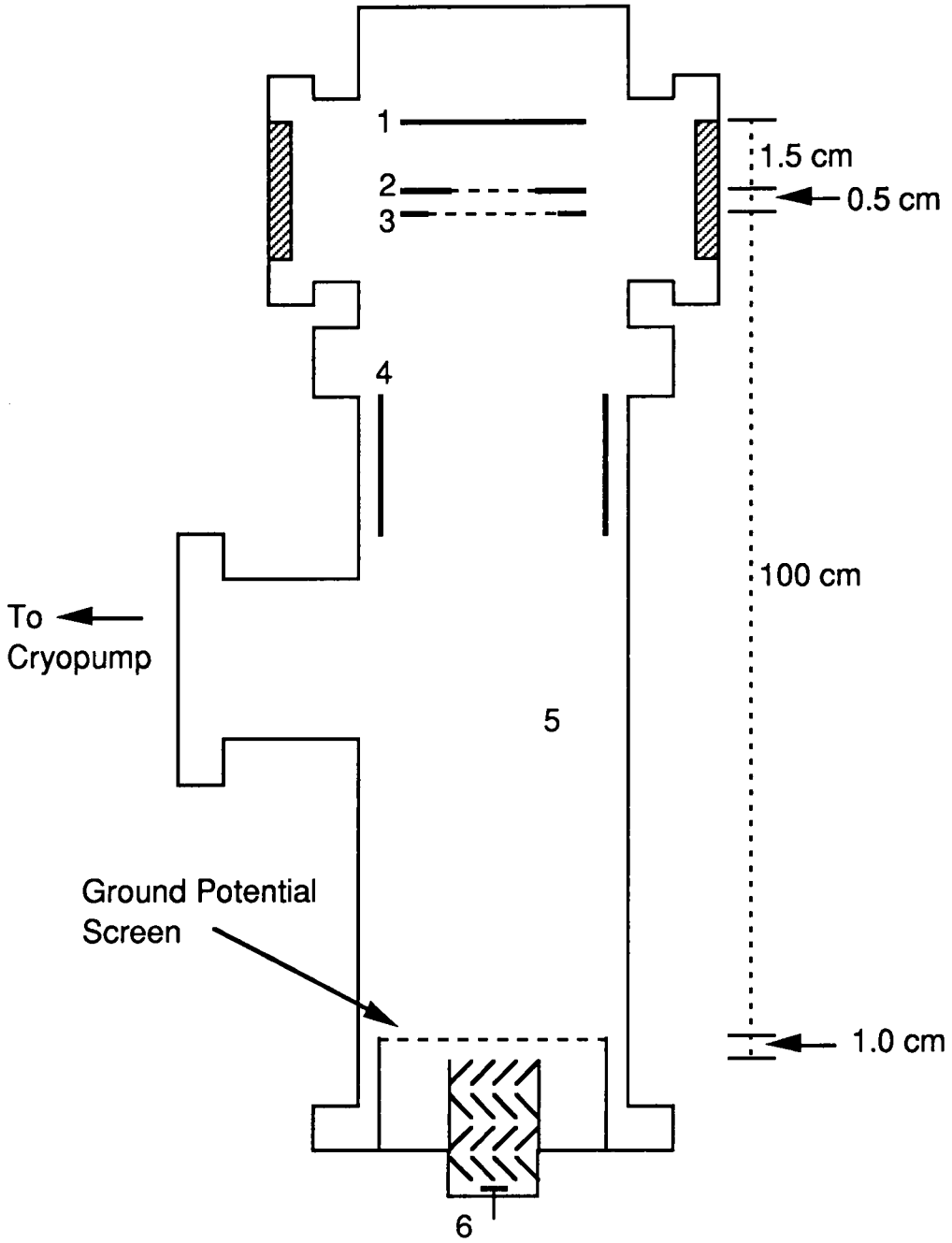

Fig. 3-1. Schematic of the time-of-flight mass spectrometer (TOF-MS). This system consists of three acceleration plates (1,2,and 3), four deflection plates (4), a field-free drift tube (5), and an electron multiplier (6).

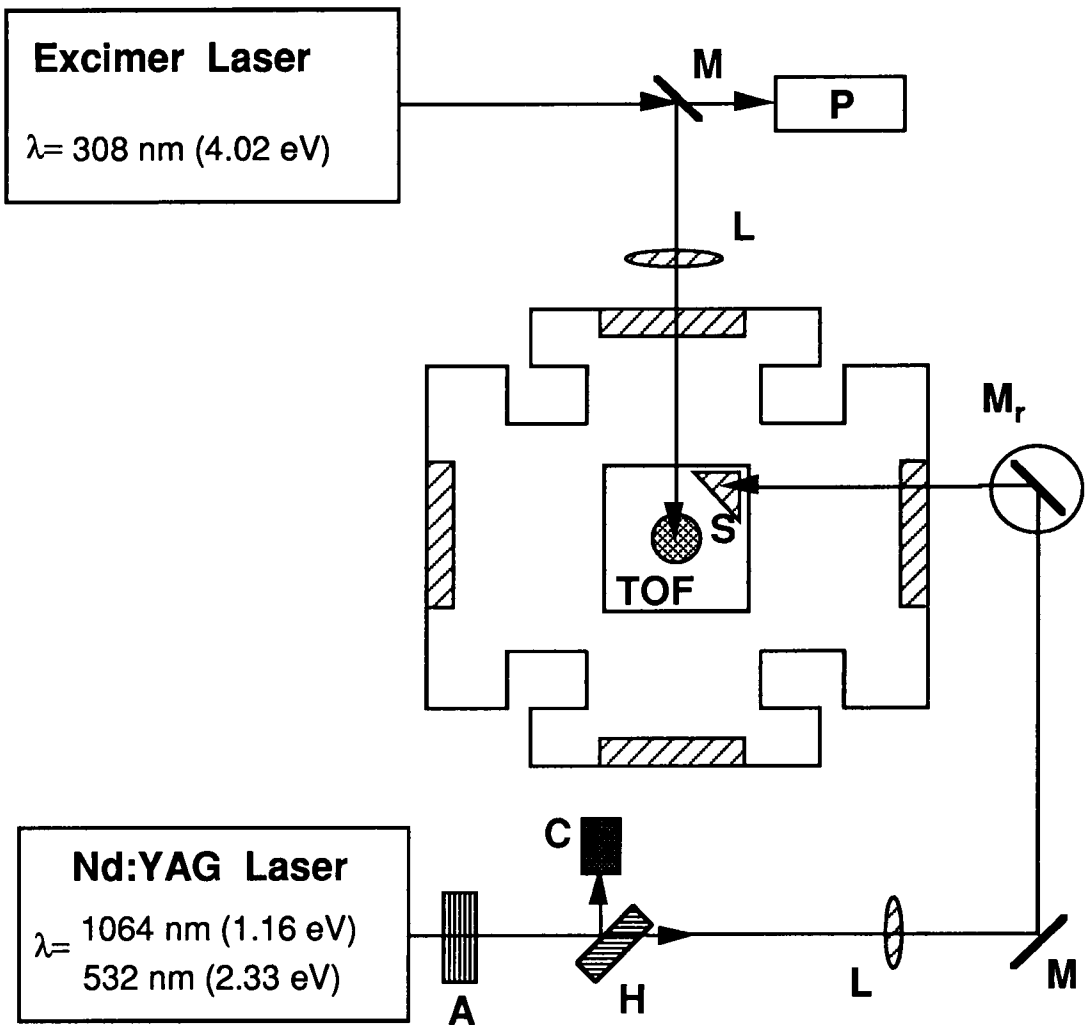

Fig. 3-2. Arrangement for desorption experiment, where A is the attenuation slides, H is the harmonic separator, C is the copper cavity, S is the metal film deposited on a glass prism, L is the focus lens for laser beam, TOF is acceleration plate of time-of-flight mass spectrometer (TOF-MS), P is the photo-diode, M is the mirror, M_r is the scanning mirror that directs the Nd:YAG laser light through the prism to the back of the metal film at different incident angles. The shaded area on the TOF plate is the aperture of acceleration plate of the TOF-MS.

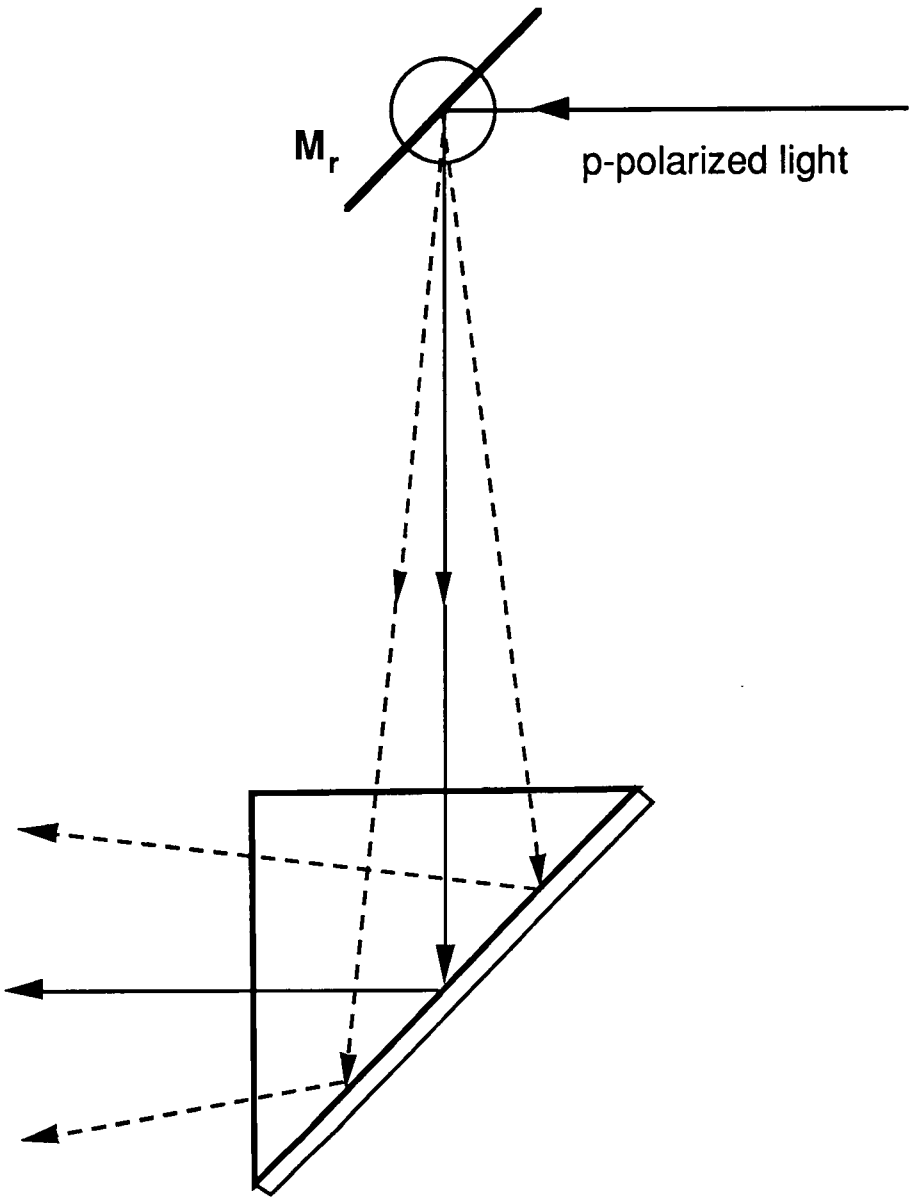

Fig. 3-3. Schematic of the ATR geometry in our experiment. The rotation of M_r varies both the incident angle and the spot position across the sample surface. This excitation geometry assures that a fresh spot is exposed at each angle.

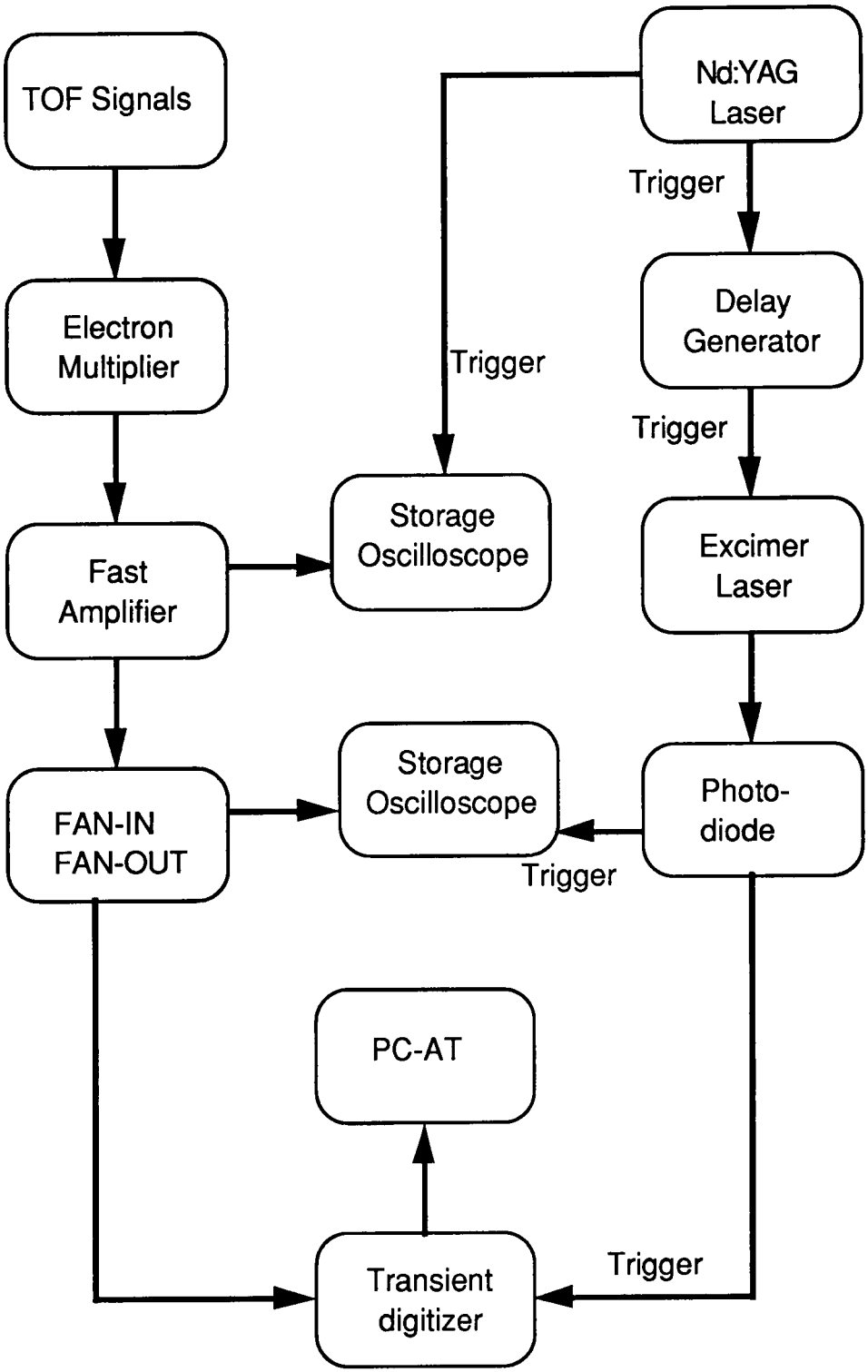

Fig. 3-4. Schematic of the data acquisition electronics.

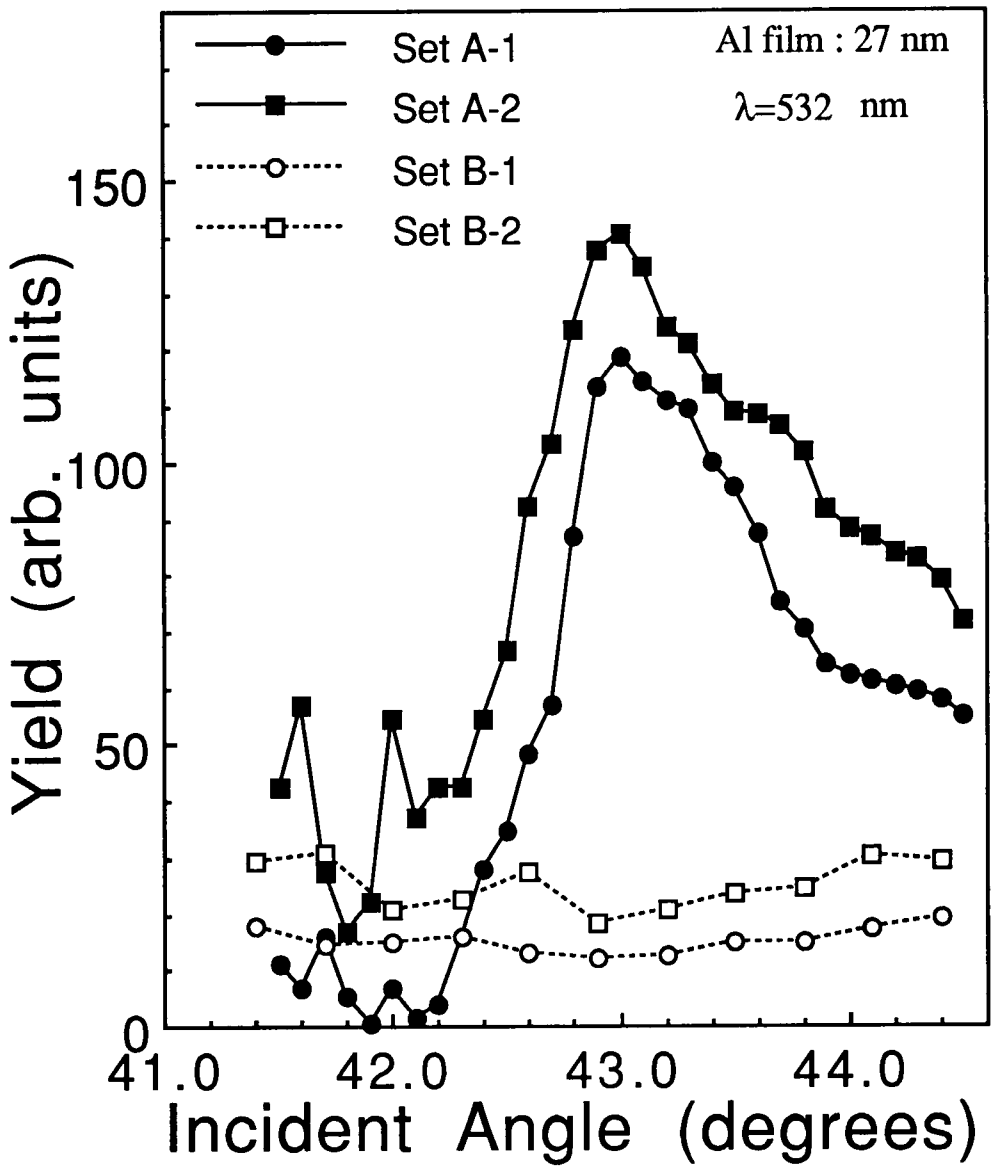

Fig. 4-1. Desorption yields from Al film at various angles of incidence. Data set A-1 and B-1 were obtained at laser fluence F = 180 mJ/cm^2. Data set A-2 and B-2 were obtained at laser fluence F = 210 mJ/cm^2. Set A-1 and A-2 are for p-polarized light through the prism. Set B-1 and B-2 are for p-polarized light directly incident upon the metal film.

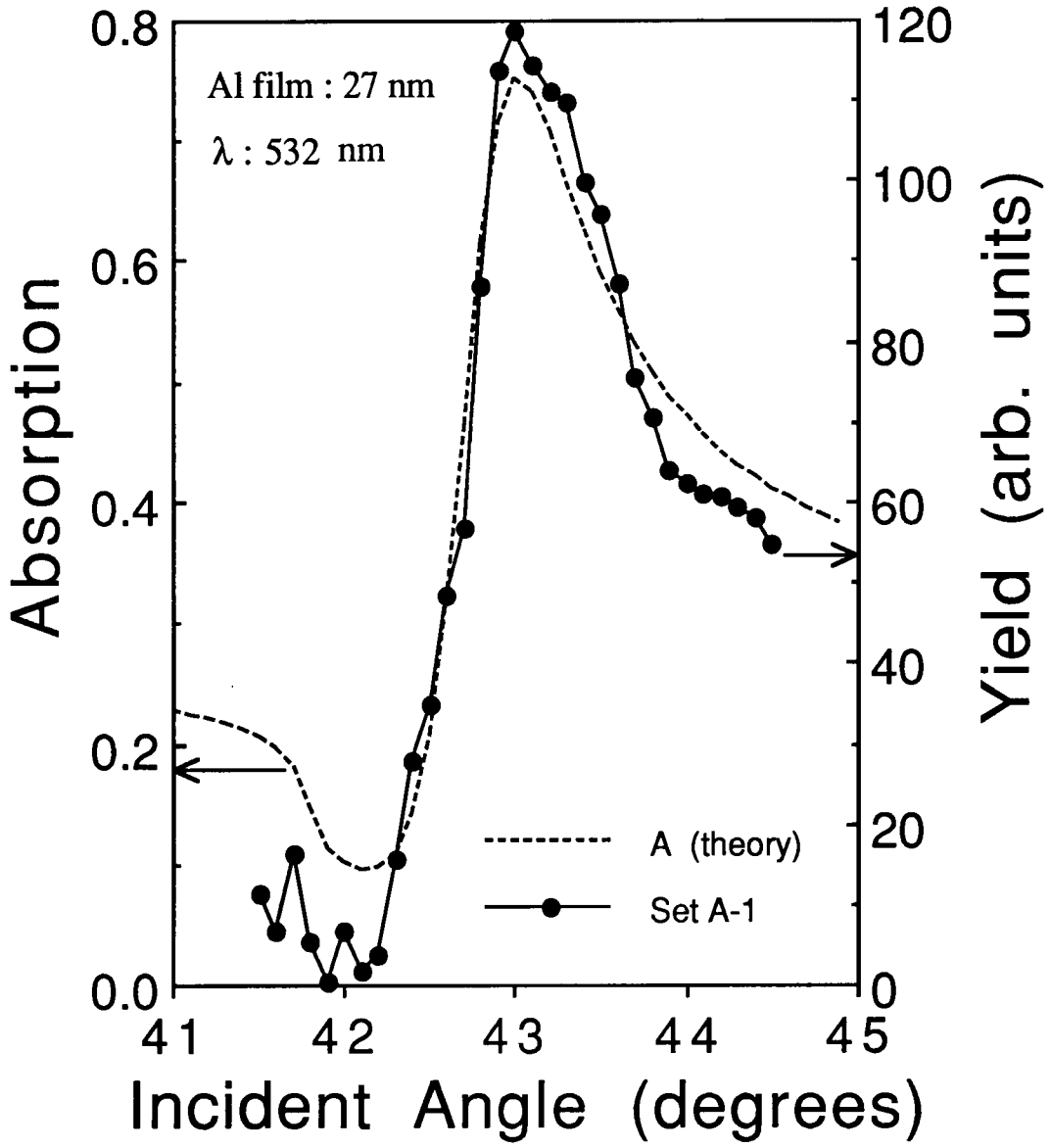

Fig. 4-2. Comparison between desorption yield A-1 and energy absorbed by the Al film at various angles.

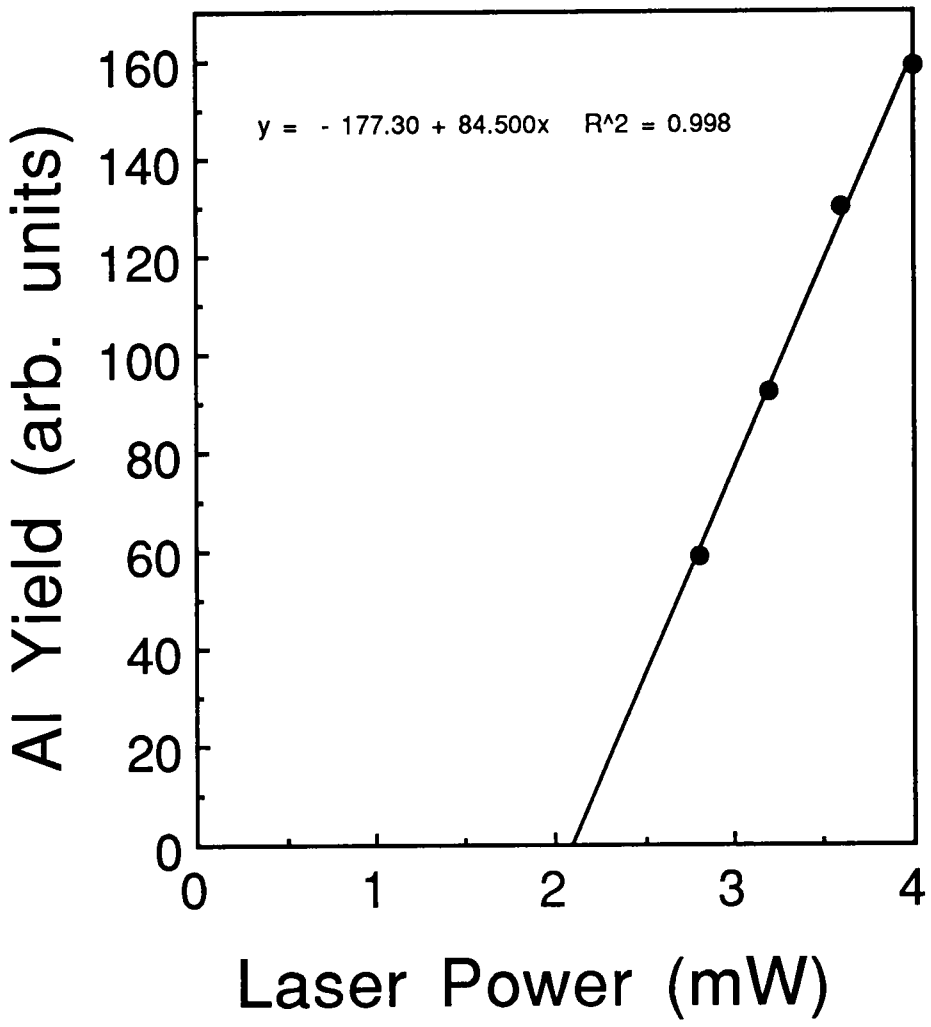

Fig. 4-3 Dependence of Al desorption yield on laser power.

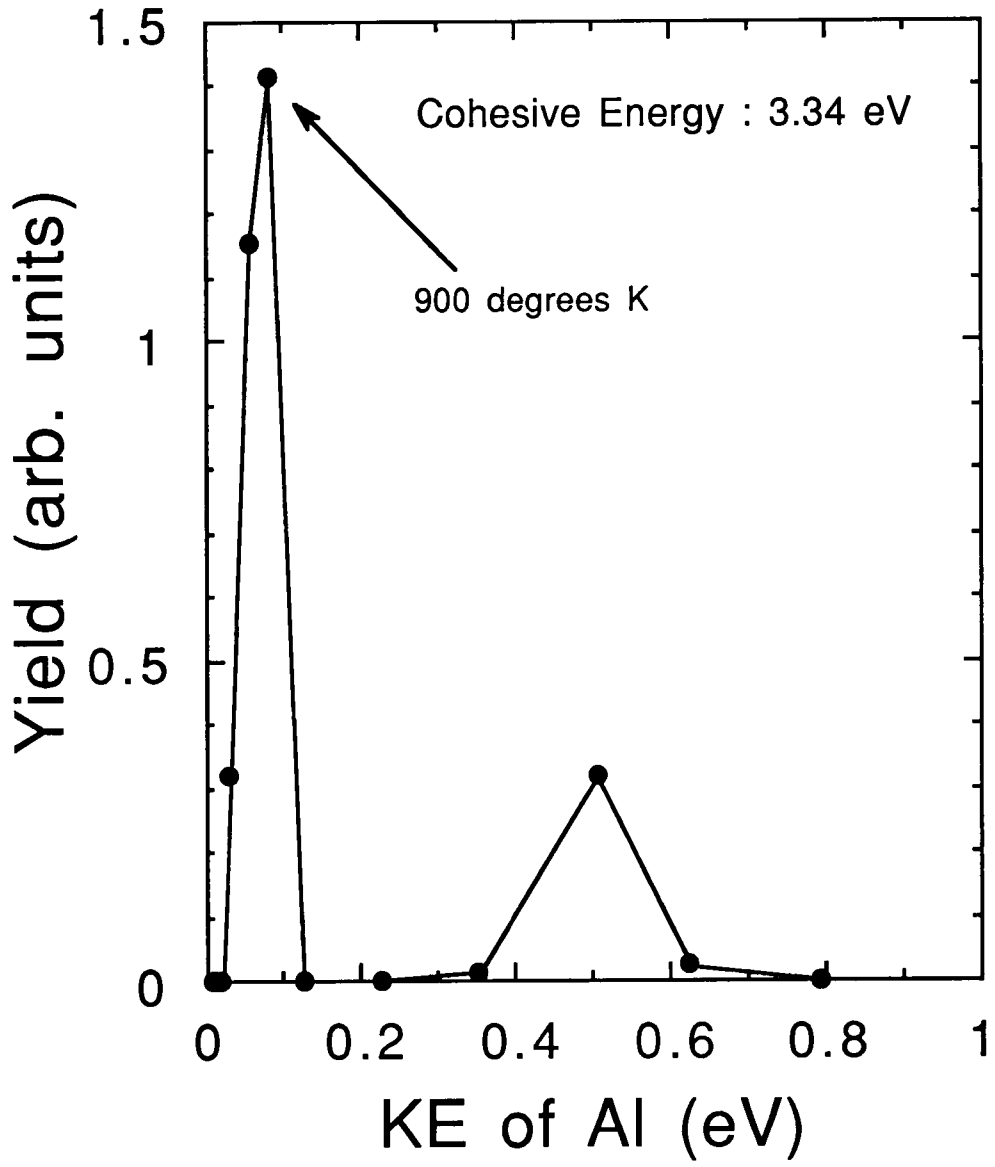

Fig. 4-4. Kinetic energy distribution of Al atoms desorbed from Al film.

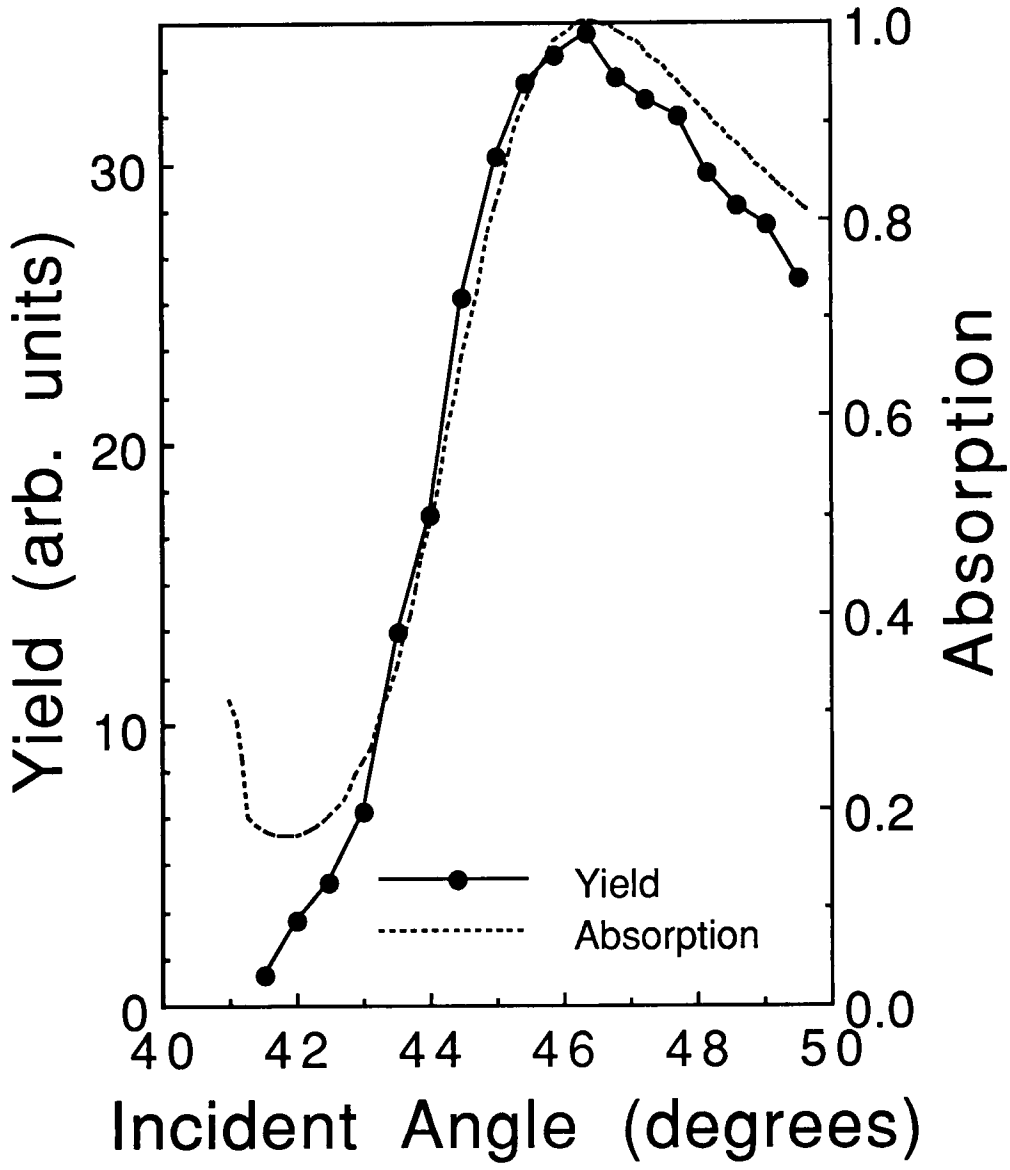

Fig. 4-5. Comparison between desorption yield from Au and calculated energy absorbed by the Au film at various angles.

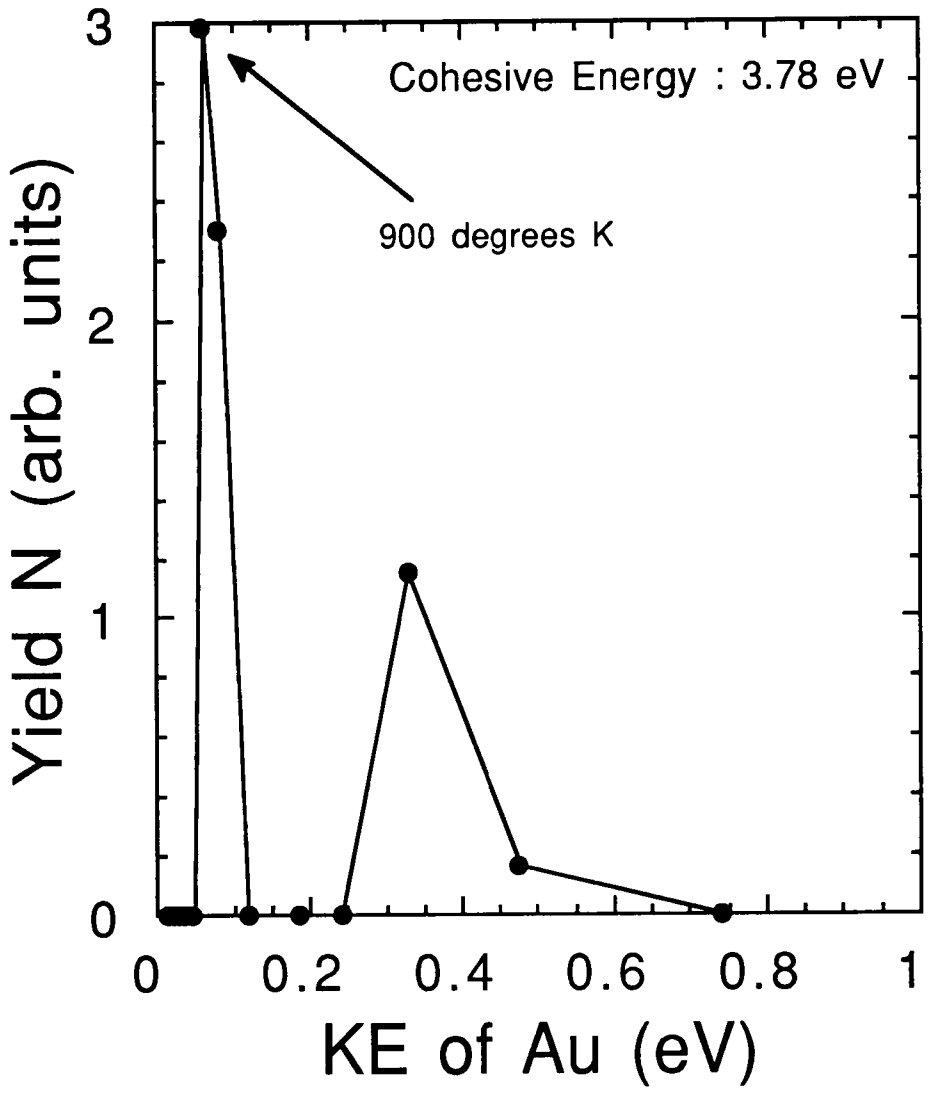

Fig. 4-6. Kinetic energy distribution of Au atoms desorbed from Au film.

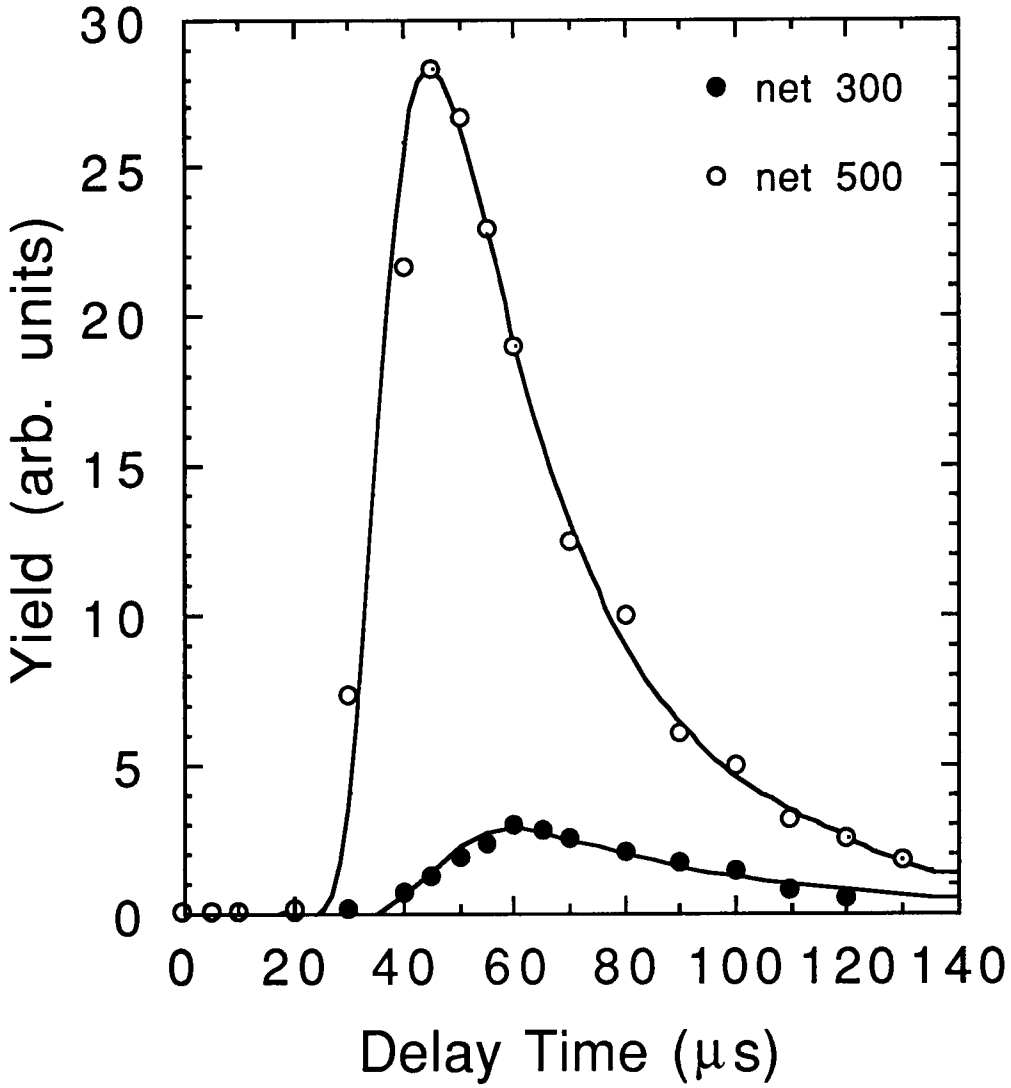

Fig. 4-7. Delay time distribution for low energy peak of Au. Where net 300 is the yield at F = 300 mJ/cm^2, and net 500 is the yield at F = 500 mJ/cm^2.

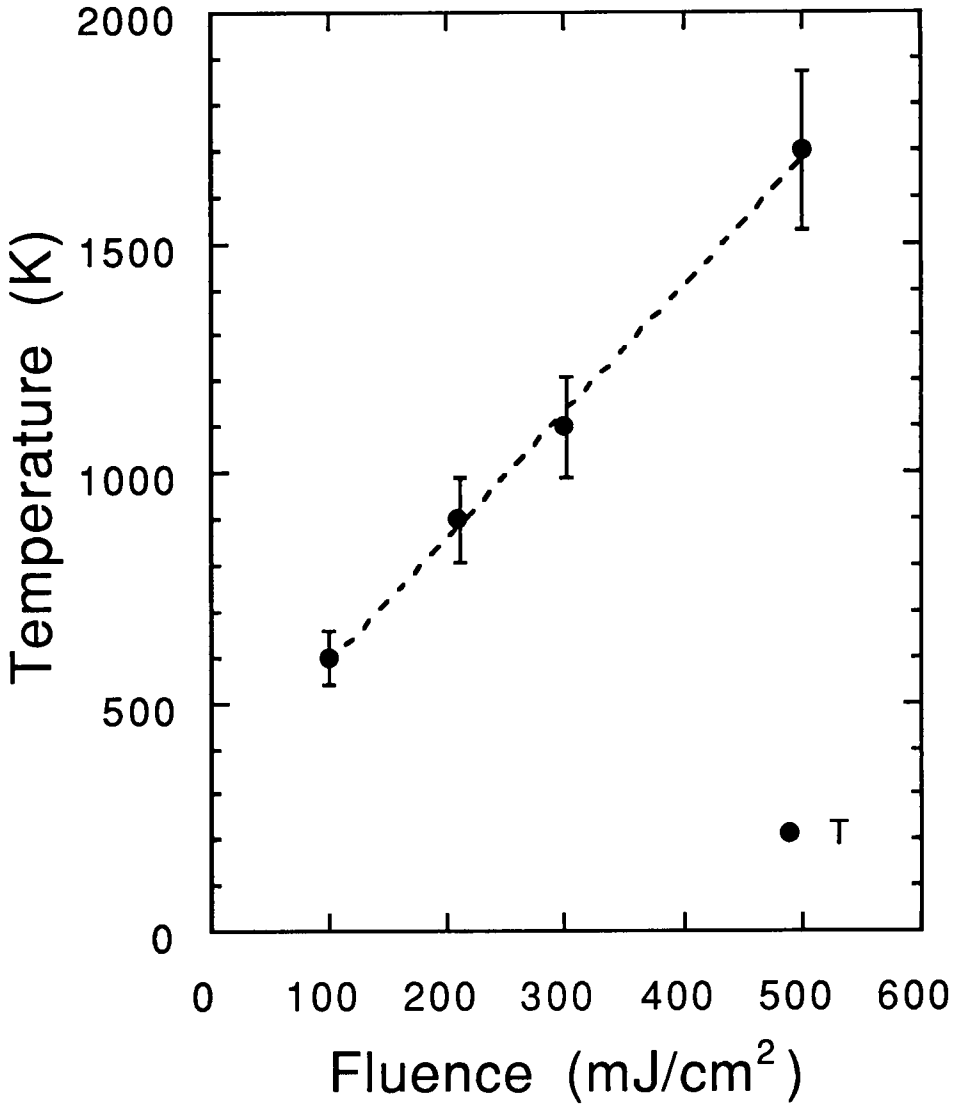

Fig. 4-8. Temperature variation of thermal peak with laser fluence.

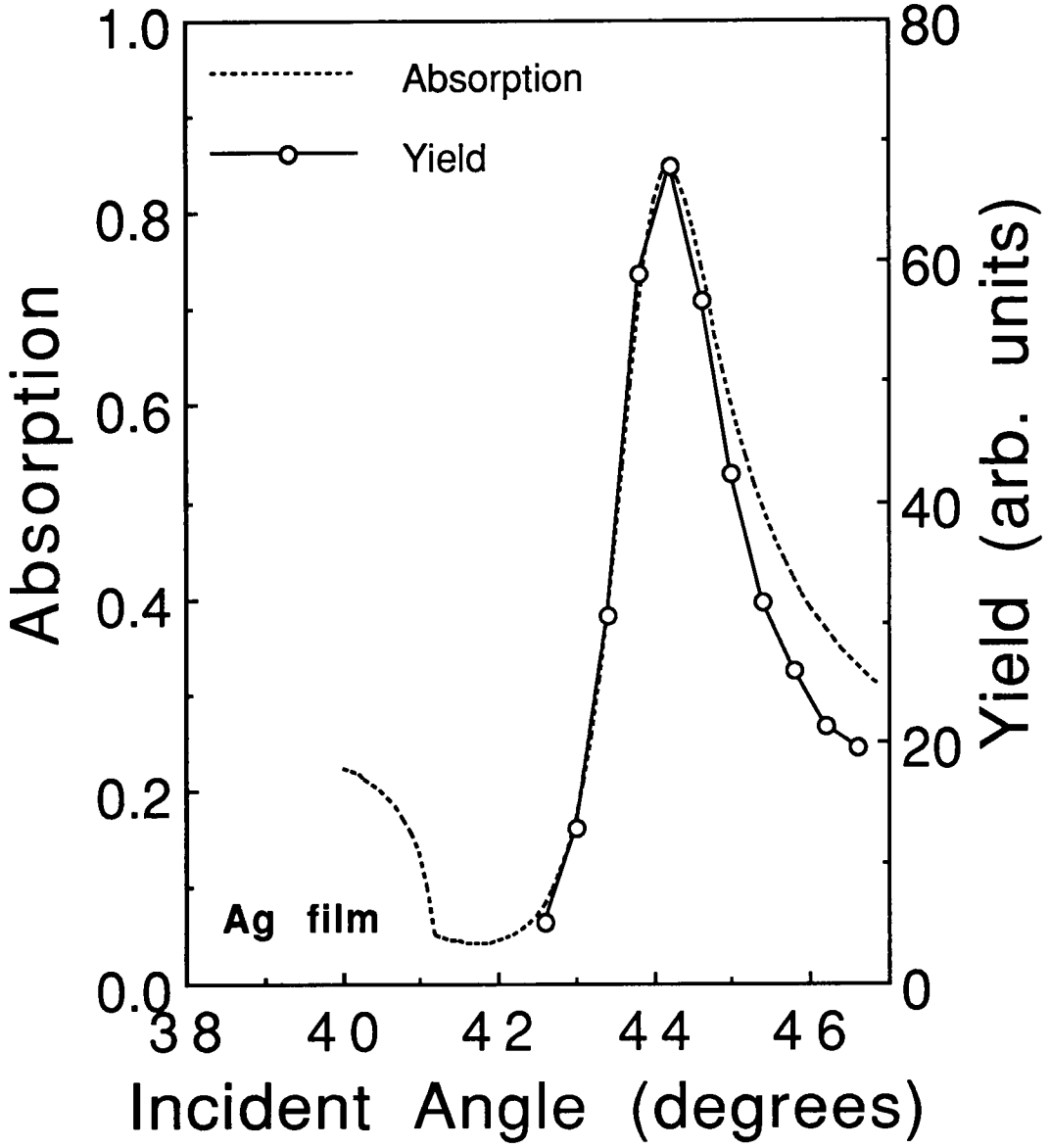

Fig. 4-9. Comparison between desorption yield from Ag and calculated energy absorbed by the Ag film at various angles.

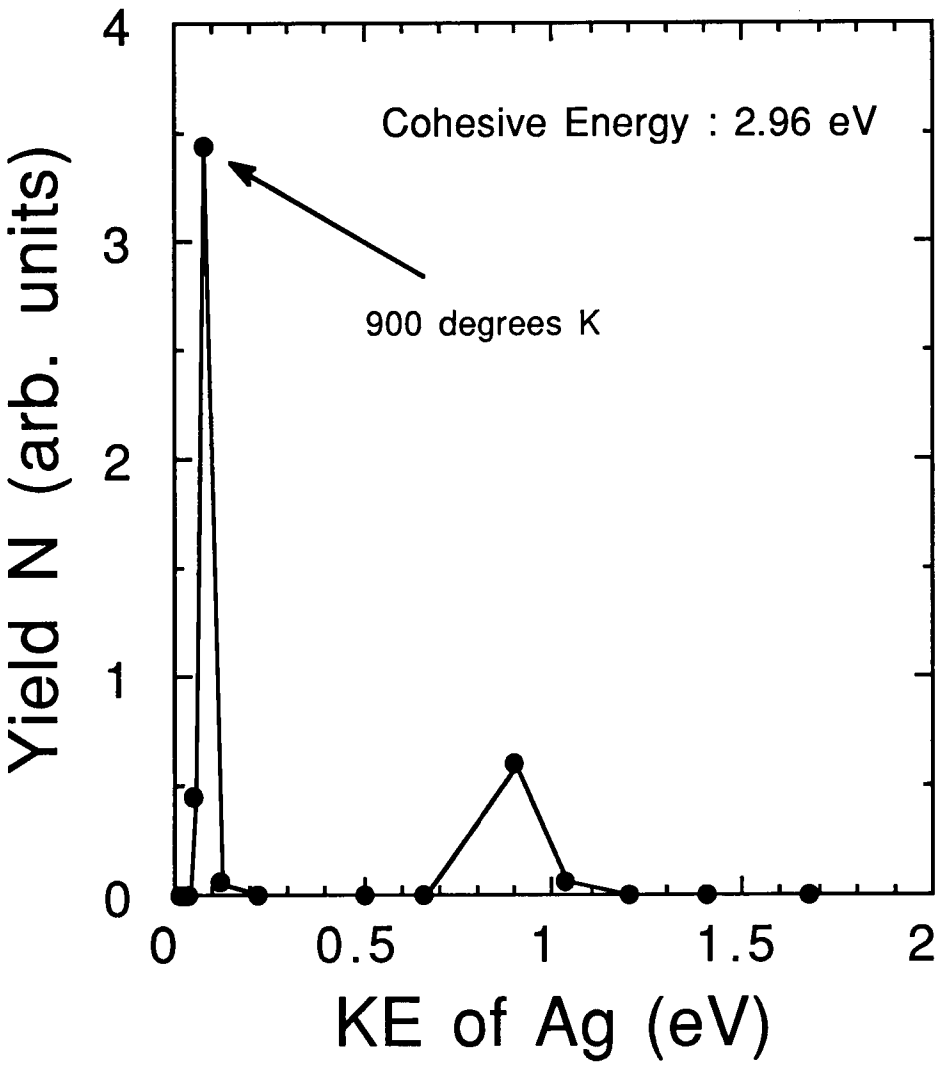

Fig. 4-10. Kinetic energy distribution of Ag atoms desorbed from Ag film.

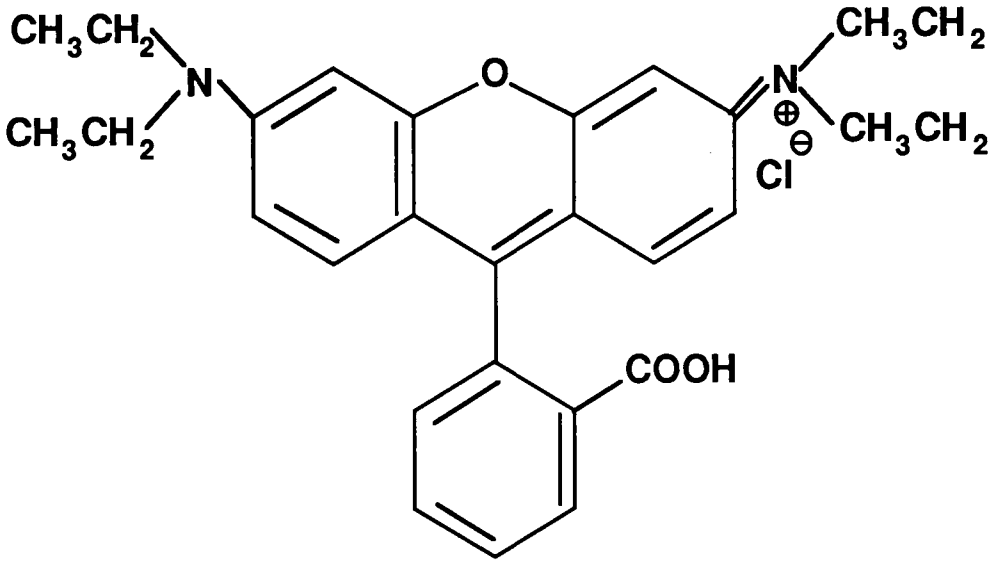

Fig. 4-11. Molecular structure of rhodamine B.

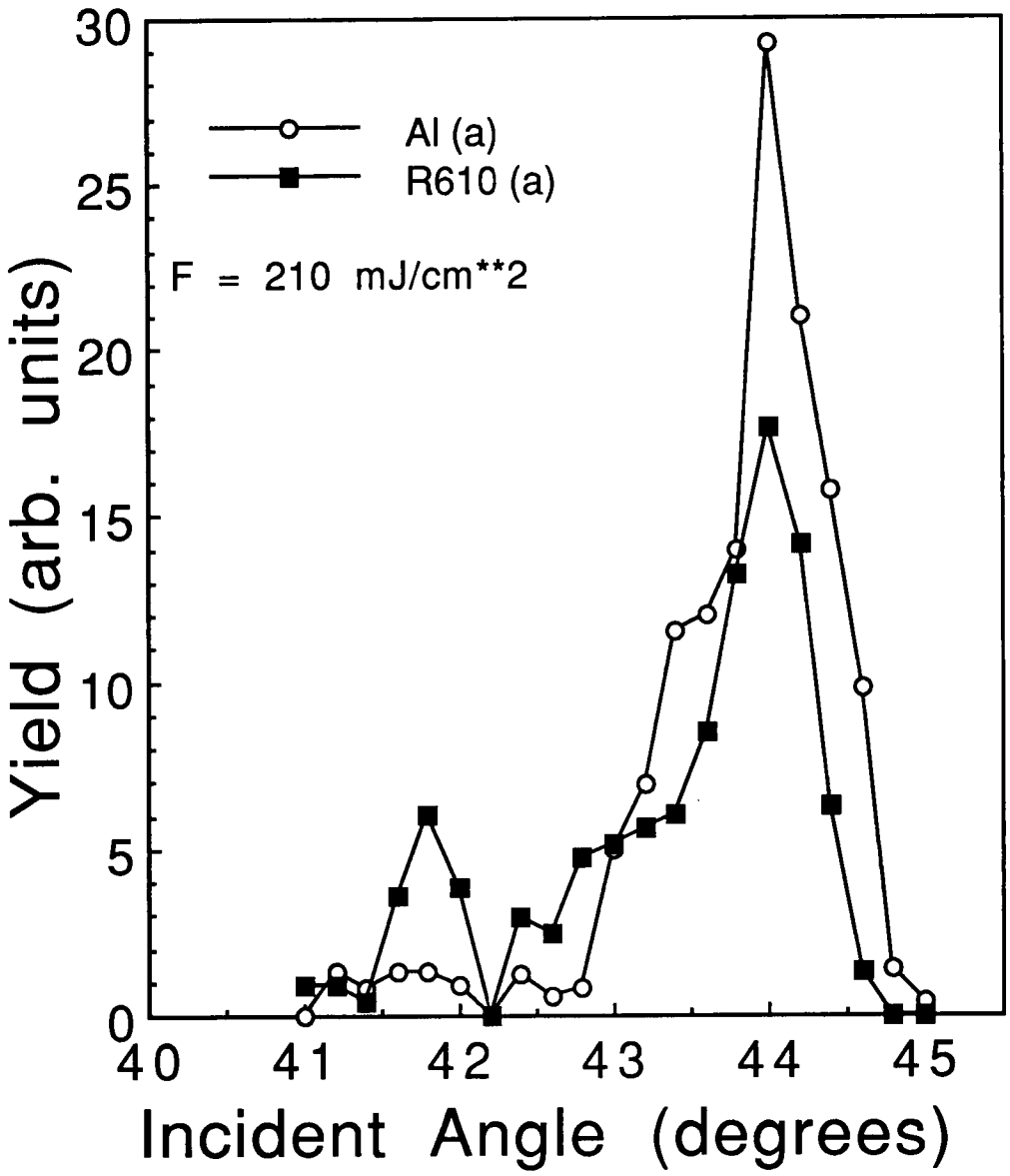

Fig. 4-12. Desorption yields from rhodamine B molecules adsorbed on an Al film at various angles of incidence with laser fluence 210 mJ/cm^2.

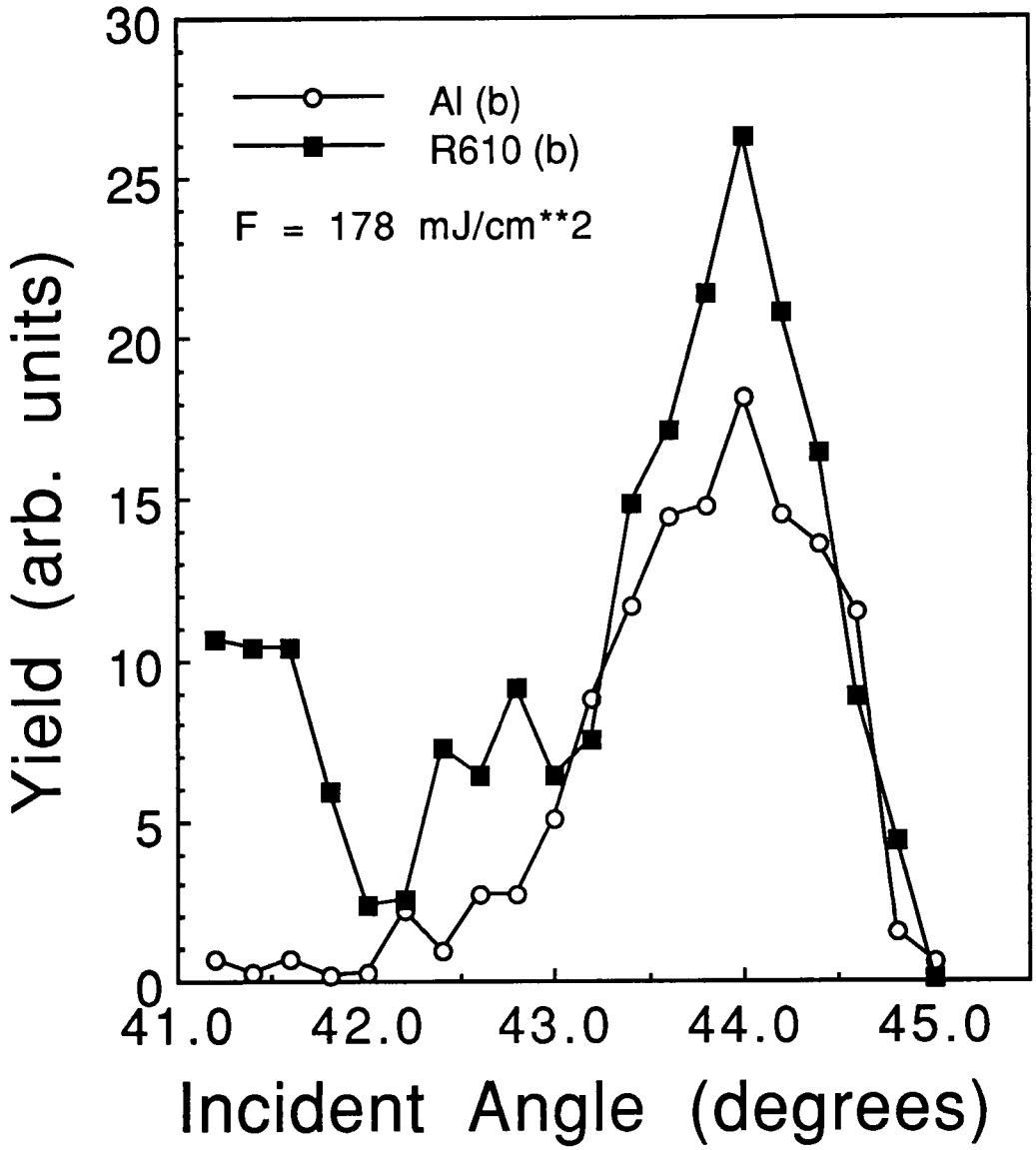

Fig. 4-13. Desorption yields from rhodamine B molecules adsorbed on an Al film at various angles of incidence with laser fluence 178 mJ/cm^2.

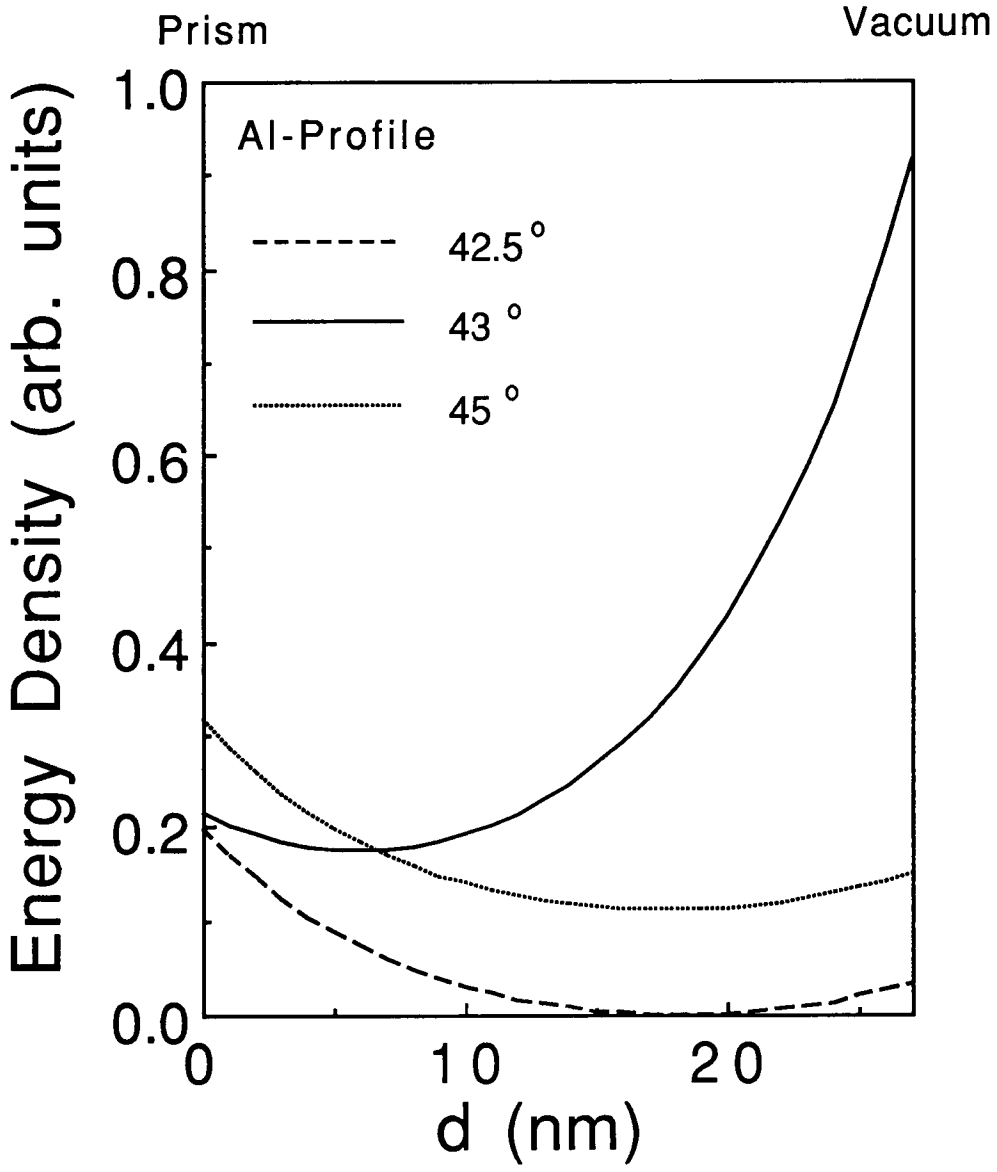

Fig. 5-1. Electromagnetic energy density profile of Al film. The plasmon resonance angle is at 43 degree.

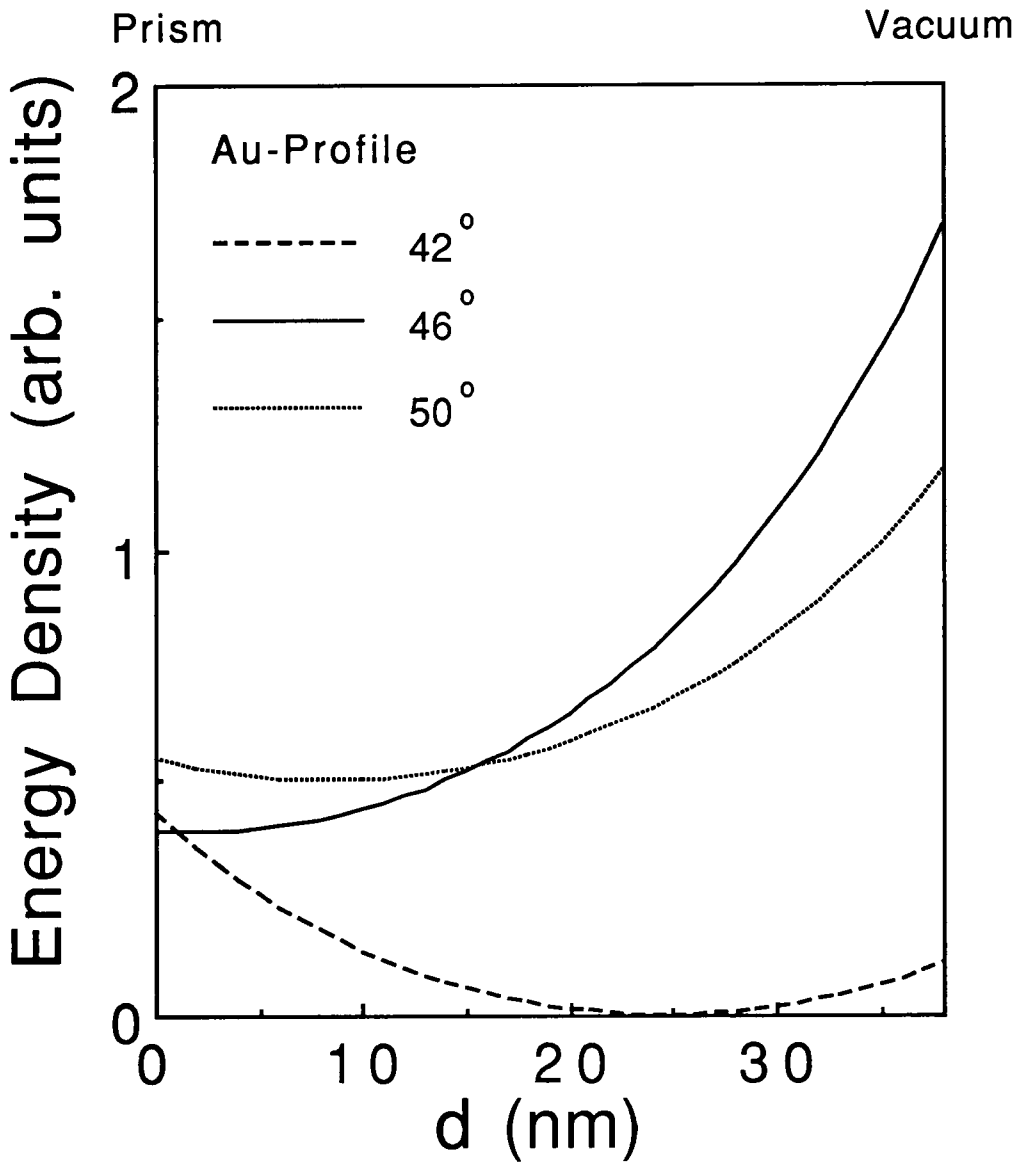

Fig. 5-2. Electromagnetic energy density profile of Au film. The plasmon resonance angle is at 46 degree.

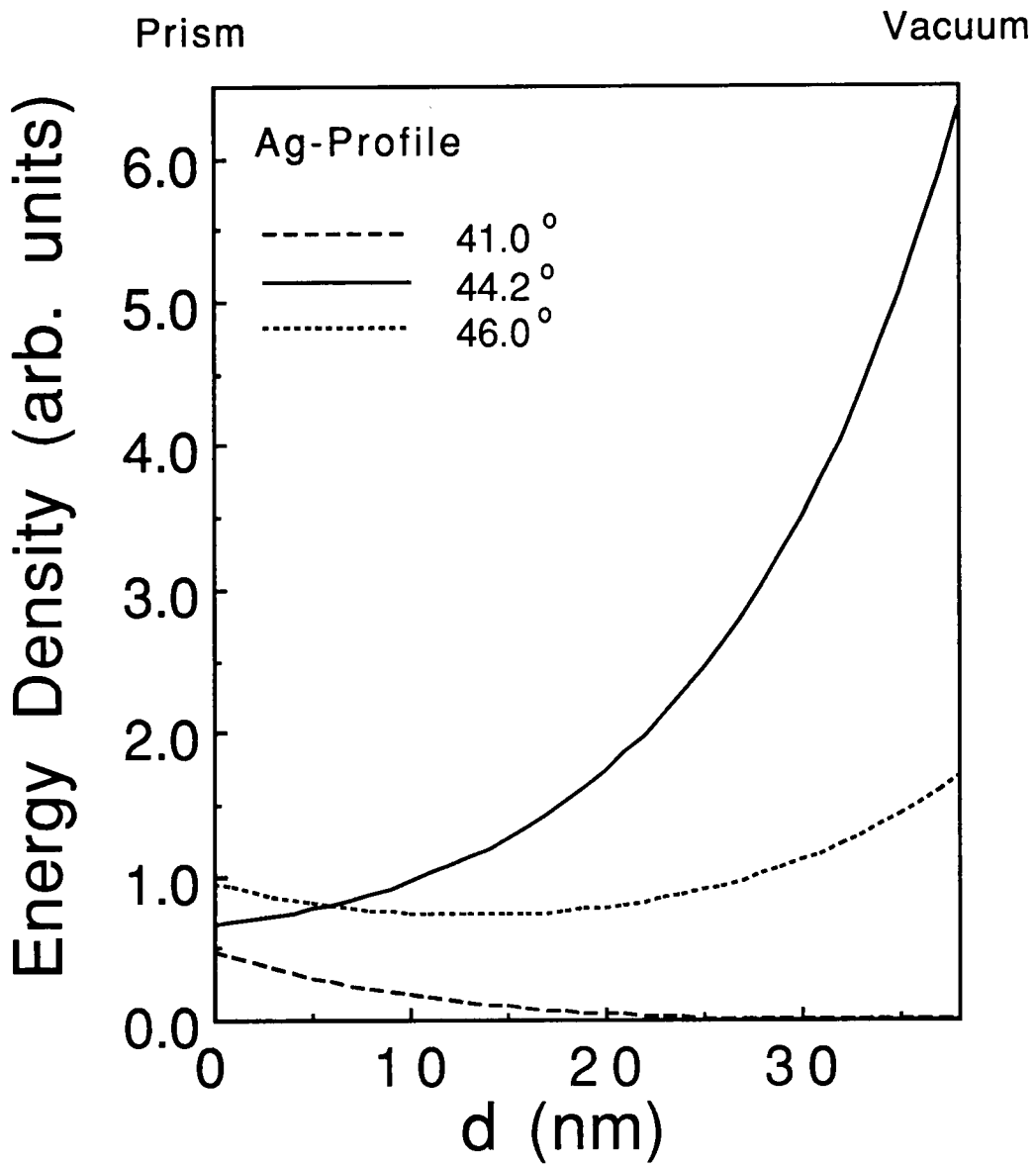

Fig. 5-3. Electromagnetic energy density profile of Ag film. The plasmon resonance angle is at 44.2 degree.

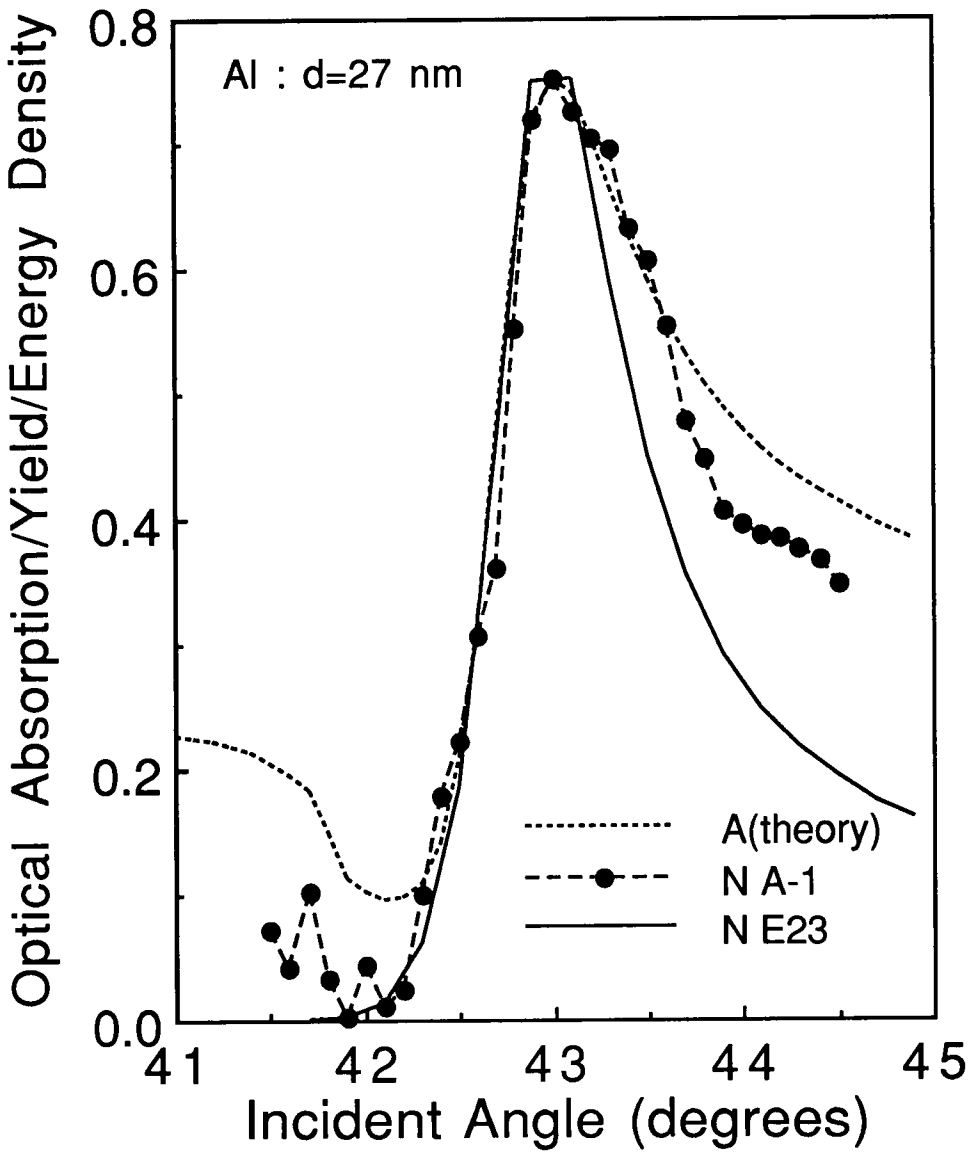

Fig. 5-4. Comparison between desorption yield, total optical absorption, and energy density at metal-vacuum interface for the Al film. A is the total optical absorption, N A-1 is the desorption yield, and N E23 is the energy density at metal-vacuum interface.

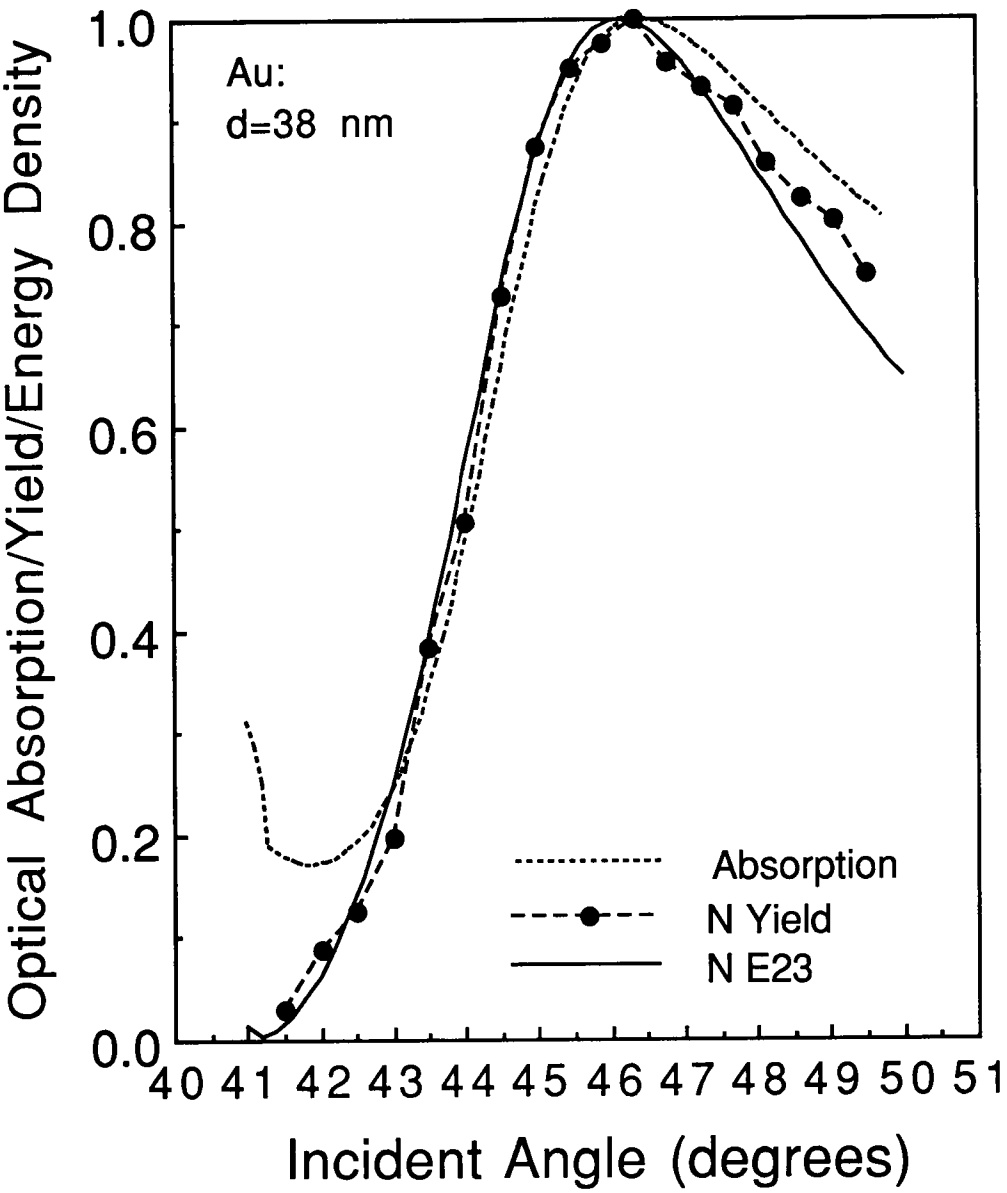

Fig. 5-5. Comparison between desorption yield, total optical absorption, and energy density at metal-vacuum interface for the Au film. Absorption is the total optical absorption, N Yield is the desorption yield, and N E23 is the energy density at metal-vacuum interface.

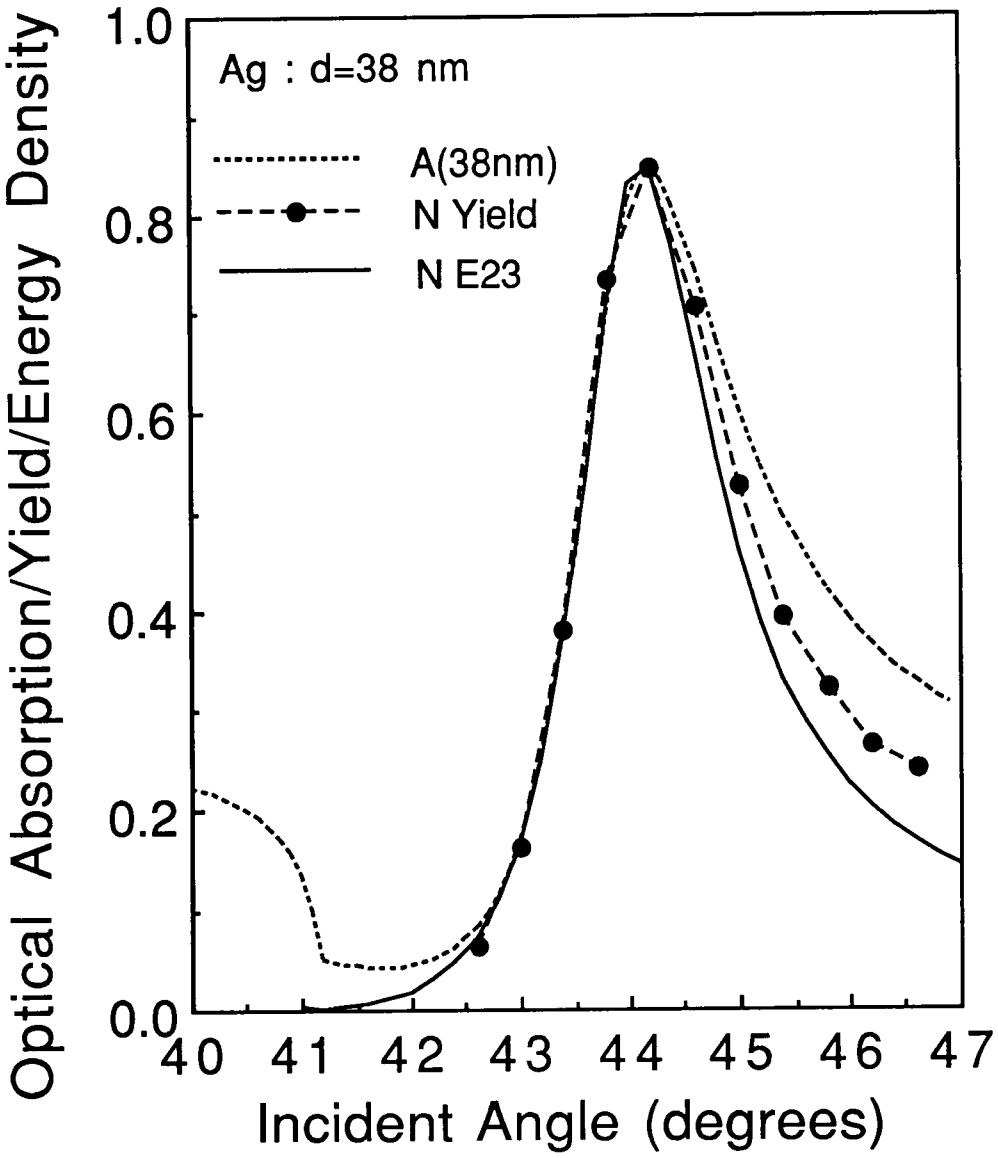

Fig. 5-6. Comparison between desorption yield, total optical absorption, and energy density at metal-vacuum interface for the Ag film. A(38 nm) is the total optical absorption, N Yield is the desorption yield, and N E23 is the energy density at metal-vacuum interface.

TABLE 3-1. LASER SPECIFICATIONS

	Desorption Laser	Ionization Laser
Type	Nd:YAG (2nd Harmonic)	Excimer (XeCl)
Manufacturer	Quanta-Ray	Lumonics
Model	DCR-1	TE861-S
Wavelength (nm)	532	308
Maximum Pulse Energy (mJ/ pulse)	70	80
Pulse Width (ns)	7	7
Average Power at 10 Hz (W)	0.7	0.8
Beam Cross Section (mm)	6.6 (diameter)	8x20
Beam Divergence (m rad full angle)	0.5	2.4x6

TABLE 3-2. ELECTRONICS LIST

	Manufacturer	Model
Fast Amplifier	LeCroy	612AM
Linear Fan-In Fan-Out	LeCroy	428F
Laser Trigger Delay Generator	Rutherford Electronics	B7B
Storage Oscilloscope	Hewlett Packard	1744A
Storage Oscilloscope	Tektronix	464
Laser Power Energy Meter	Scientech	362
High Voltage Power Supply	ORTEC	456
High Voltage Power Supply	Bertan	315

TABLE 5-1. ENERGIES OF DESORBED PARTICLES

	Threshold	Kinetic Energies / Momentum	
		Thermal	Nonthermal
	(mJ/cm^2)	(eV) / (10^{-3} eV s/m)	(eV) / (10^{-3} eV s/m)
Al	100	0.081 / 0.21	0.50 / 0.53
Au	100	0.082 / 0.58	0.33 / 1.16
Ag	100	0.081 / 0.43	0.90 / 1.43
Rh.*	80	None	0.56 / 2.37
Si	(Same as for metal films)	0.083 / 0.22	None

* Rh. : rhodamine B molecules.

REFERENCES

[1] I.W. Boyd, Laser Processing of Thin Films and Microstructures (Springer-Verlag, New York, 1987).

[2] F. A. Houle, Appl. Phys. A41 (1986) 315.

[3] J.B. Pallix, C.H. Becker, and N. Newman, J. Vac. Sci. Technol. A6 (1988) 1049.

[4] C.H. Becker and J.B. Pallix, J. Appl. Phys. 64 (1988) 5152.

[5] C.H. Chen, M.P. McCann, and R.C. Phillips,Bull. Am. Phys. Soc.34, No. 7 (1989) 1679.

[6] T.T. Tsong, Phys. Rev. B30 (1984) 4946.

[7] R. Tembreull and D.M. Lubman, Anal. Chem. 58 (1986) 1299.

[8] H. Zacharias, Appl. Phys. A47 (1988) 37.

[9] T.J. Chuang, Surf. Sci. Rep. 3 (1983) 1.

[10] T.J. Chuang, J. Vac. Sci. Technol. B3 (1985) 1408.

[11] T.J. Chuang, Surf. Sci. 158 (1985) 525.

[12] T.J Chuang, Surf. Sci. 178 (1986) 763.

[13] H. Zacharias, Appl. Phys. A47 (1988) 37.

[14] G.Wedler and H. Ruhmann, Surf. Sci. 121 (1982) 464.

[15] D.R. Burgess, Jr., R. Viswanathan, I. Hussla, P.C. Stair, and E. Weitz, J. Chem. Phys. 79 (1983) 5200.

[16] B. Schafer and P. Hess, Appl. Phys. B37 (1985) 197.

[17] I. Hussla, H. Coufal, F. Trager, and T.J. Chuang, Ber. Bunsenges. Phys. Chem. 90 (1986) 240.

[18] P.C. Stair and E. Weitz, J. Opt. Soc. Am. B4 (1987) 255.

[19] J. Heidberg, H. Stein, and E. Riehl, Phys. Rev. Lett. 49 (1982) 666.

[20] J. Heidberg, H. Stein, E. Riehl, Z. Szilagyi, and H. Weiss, Surf. Sci. 158 (1985) 525.

[21] T. J. Chuang, Surf. Sci. 158 (1985) 525.

[22] Z.W. Gortel, H.J. Kreuzer, P. Piercy, and R. Teshima, Phys. Rev. B27 (1983) 5066.

[23] V.S. Antonov, V.S. Letokhov, and A.N. Shibanov, Appl. Phys. 25 (1981) 71.

[24] E.B.D. Bourdon, J.P. Cowin, I. Harrison, J.C. Polanyi, J. Segner, C.D. Stanners, and P.A. Young, J. Phys. Chem. 88 (1984) 6100.

[25] K. Domen, and T.J. Chuang, Phys. Rev. Lett. 59 (1987)1484.

[26] F. Budde, A.V. Hamza, P.M. Ferm, and G. Ertl, Phys. Rev. Lett. 60 (1988) 1518.

[27] J.F. Ready, Effects of High-Power Laser Radiation (Academic Press, New York, 1971).

[28] M. von Allmen, Laser-Beam Interactions with Materials (Springer-Verlag, New York, 1987).

[29] D.S. Kliger, Ultrasensitive Laser Spectroscopy (Academic Press, New York, 1983) .

[30] T.J. Chuang, and K. Domen, J. Vac. Sci. Technol. A5 (1987) 473.

[31] T.A. Germer, and W. Ho, J. Chem. Phys. 89 (1988) 562.

[32] Y. Zhou, W.M. Feng, M.A. Henderson, B. Roop, and J.M. White, J. Am. Chem. Soc. 110, (1988) 4447.

[33] S.A. Buntin, L.J. Richter, R.R. Cavangh, and D.S. King, Phys. Rev. Lett. 61 (1988) 1321.

[34] E.P. Marsh, T.L. Gilton, W. Meier, M.R. Schneider, and J.P. Cowin, Phys. Rev. Lett. 61 (1988) 2725.

[35] T.J. Chuang, H. Hiraoka, and A. Modl, Appl. Phys. A45 (1988) 277.

[36] H. Helvajian, and R. Welle, J. Chem. Phys. 91 (1989) 2616.

[37] W. Hoheisel, K. Jungmann, M. Vollmer, R. Weidenauer, and F. Trager, Phys. Rev. Lett. 60 (1988) 1649.

[38] W. Hoheisel, U. Schulte, M. Vollmer, R. Weidenauer, and F. Trager, Appl. Surf. Sci. 36 (1989) 664.

[39] R. Weidenauer, M. Vollmer, W. Hoheisel, U. Schulte, and F. Trager, J. Vac. Sci. Technol. A7 (1989) 1972.

[40] V.S. Letokhov, V.G. Movshev, and S.V. Chekalin, Sov. Phys. JEPT 54 (1981)257.

[41] V.G. Movshev and S.V. Chekalin, Sov. J. Quantum Electron. 13 (1983) 925.

[42] S.V. Chekalin, V.S. Letokhov, V.S. Likhachev, and V.G. Movshev, Appl. Phys. B33 (1984) 57.

[43] I. Lee, J.E. Parks II, T.A. Callcott, and E.T. Arakawa, Phys. Rev. B39 (1989) 8012.

[44] D. Bohm and D. Pines presented a three-part description of collective electron interactions : Part I, Phys. Rev. 82 (1951) 625; Part II, Phys. Rev. 85 (1952) 338 ; and Part III, Phys. Rev. 92 (1953) 609; D. Pines, Phys. Rev. 92 (1953) 626.

[45] R.H. Ritchie, Phys. Rev. 106 (1957) 874.

[46] H. Raether, Surface Plasmons on Smooth and Rough Surfaces and on Gratings (Springer-Verlag, New York, 1988).

[47] K. Kretschmann, Z. Physik 241 (1971) 313.

[48] J.F. Ready, Effects of High-Power Laser Radiation (Academic Press, New York, 1971) pp. 110.

[49] B.Lindner and U. Seydel, Anal. Chem. 57 (1985) 895.

[50] R.A. Rosenberg, and C. Wen, Phys. Rev. B39 (1989) 6630.

[51] J.C. Tully, Surface Sci. 111 (1981)461.

[52] R.R.Lucchese and J.C. Tully,J. Chem. Phys. 81 (1984)6313.

[53] R.B.Hall and A. M. DeSantolo, Surface Sci. 137 (1984) 421.

[54] P.C. Stair and Eric Weitz, J. Opt. Soc. Am B4 (1987) 255.

[55] R.N. Zare and R.D. Levine, Chem. Phys. Lett. 136 (1987) 593.

[56] Z.W. Gortel, H.J. Kreuzer, P. Piercy, and R. Teshima, Phys. Rev.B28 (1983) 5066.

[57] I. Hussla, H. Seki, T.J. Chuang, Z.W. Gortel, H.J. Kreuzer, and P. Piercy, Phys Rev. B32 (1985) 3489.

[58] J. Lin and T.F. George, Surface Sci. 115 (1982) 569.

[59] H.J. Kreuzer, Z.W. Gortel, and P. Piercy, J. Opt. Soc. Am. B4 (1987) 248.

[60] S.H. Lin, A. Boeglin, and B. Fain, J. Opt. Soc. Am. B4 (1987) 211.

[61] W.H. Weber and G.W. Ford, J. Opt. Soc. Am. B4 (1987) 261.

[62] D. Menzel and R. Gomer, J. Chem. Phys. 41 (1964) 3311.
P.A. Redhead, Can. J. Phys. 42 (1964) 886.

[63] M.L. Knotek and P.J. Feibelman, Phys. Rev. Lett. 40 (1978) 964;
P.J. Feibelman and M.L. Knotek, Phys. Rev. B18 (1978) 6531.

[64] Z. Wu, Phys. Lett. A 131 (1988) 486;
L. Chen, V. Liberman, J.A. O'Neill, Z. Wu, and R.M. Osgood,Jr., J. Vac. Sci. Technol. A6 (1988) 1426.

[65] D.M. Lubman, Lasers and Mass Spectrometry (Oxford University Press, New York, 1990).

[66] V.S. Letokhov, Laser Photoionization Spectroscopy (Academic Press, New York, 1987).

[67] N.S. Nogar, Laser Photoionization and Desorption Surface Analysis Techniques (SPIE, Washington,1990).

[68] C.H. Becker and K.T. Gillen, Anal. Chem. 56 (1984) 1671.

[69] C.H. Becker and K.T. Gillen, J. Opt. Soc. Am. B2 (1985) 1438.

[70] D.W. Beekman, Development of Time-of-Flight Mass Spectrometer with Laser Microprobe and Multiphoton Resonance Ionization (Dissertation, The university of Tennessee, Knoxville, 1983) pp. 21.

[71] M.A. Ordal, L.L. Long, R.J. Bell, S.E. Bell, R.R. Bell, R.W. Alexander, Jr., and C.A. Ward, Appl. Opt. 22 (1983) 1099.

[72] N.S. Nogar, R.C. Estler, and C.M. Miller, Anal. Chem. 57 (1985) 2441.

[73] M.M. Timoshenko, I.V. Korkoshko, V.I. Kleimenov, N.E. Petrachenko, Y.V. Chizhov, V.V. Rylkov, and M.E. Akopyan, Doklady Physical Chemistry (Consultants Bureau, New York, 1982) pp. 800.

[74] R. Tembreull and D. Lubman, Anal. Chem. 58 (1986) 1299.

[75] D. M. Lubman, Anal. Chem. 59 (1987) 31A.

[76] J.F. Ready, Effects of High-Power Laser Radiation (Academic Press, New York, 1971) pp. 109.

[77] F. Neuman, Appl. Phys. Lett. 4 (1964)167.

[78] H.P. Steinruck, K.D. Rendulic, and A. Winkler, Surf. Sci. 29 (1985) 99.

[79] H.P. Steinruck, A. Winkler, and , K.D. Rendulic, Surf. Sci. 152/153 (1985) 323.

[80] K.D. Rendulic, Appl. Phys. A47 (1988) 55.

VITA

Ida Lee was born in Taipei, Taiwan, Republic of China. She attended elementary school in that city and wanted to be a scientist since then. In June 1980 she received a Bachelor of Science degree in Physics at The Tunghai University in Taiwan.

In September 1980 she began graduate studies at The University of Tennessee in Knoxville. Research on her dissertation project began at Oak Ridge National Laboratory in December 1984, leading to the Doctor of Philosophy degree in Physics. Her wish finally came true at the end of 1990.